Diindolocarbazole – Achieving Multiresonant Thermally Activated Delayed Fluorescence Without The Need for Acceptor Units

David Hall,[a, b] Kleitos Stavrou,[c] Eimantas Duda,[d] Andrew Danos,[c] Sergey Bagnich,[d] Stuart Warriner,[e] Alexandra M. Z. Slawin,[a] David Beljonne,[b] Anna Köhler,[d]* Andrew Monkman,[c]* Yoann Olivier,[f]* and Eli Zysman-Colman[a]**

[a]Organic Semiconductor Centre, EaStCHEM School of Chemistry, University of St Andrews, St Andrews, UK, KY16 9ST. E-mail: eli.zysman-colman@st-andrews.ac.uk; http://www.zysman-colman.com

[b]Laboratory for Chemistry of Novel Materials, University of Mons, 7000, Mons, Belgium.

[c]Department of Physics, Durham University, Durham, UK, DH1 3LE. Email: a.p.monkman@durham.ac.uk

[d]Soft Matter Optoelectronics, BIMF & BPI, University of Bayreuth, Universitätsstraße 30, 95447 Bayreuth, Germany. E-mail: anna.koehler@uni-bayreuth.de

[e] School of Chemistry, University of Leeds, Woodhouse Lane, Leeds, UK

[f]Laboratory for Computational Modeling of Functional Materials & Solid State Physics Laboratory, Namur Institute of Structured Matter, University of Namur, Rue de Bruxelles, 61, 5000 Namur, Belgium. E-mail: yoann.olivier@unamur.be

SUPPORTING INFORMATION

Table of Contents

General methods

General Synthetic Procedures. All commercially available chemicals and reagent grade solvents were used as received. Solvents used in the reactions were dry and deaerated using an MBRAUN solvent purification system. Air-sensitive reactions are done under a nitrogen atmosphere using Schlenk techniques. Flash column chromatography was carried out using silica gel (Silia-P from Silicycle, 60 Å, 40-63 µm). Analytical thin-layer-chromatography (TLC) was performed with silica plates with aluminium backings (250 µm with F-254 indicator). TLC visualization was accomplished by use of a 254/365 nm UV lamp. HPLC analysis was conducted on a Shimadzu Prominence Modular HPLC system. HPLC traces were performed using an ACE Excel 2 C18 analytical column in THF and MeOH. ^{1}H and ^{13}C and NMR spectra were recorded on a Bruker Advance spectrometer (500 MHz for ^{1}H and 125 MHz for ^{13}C). The following abbreviations have been used for multiplicity assignments: “s” for singlet, “d” for doublet, “t” for triplet, “dd” for doublet of doublets, “ddd” for doublet of doublet of doublets and “m” for multiplet. Deuterated chloroform ($CDCl_3$) and deuterated DMSO (DMSO-d_6) was used as the solvents of record. ^{1}H and ^{13}C NMR spectra were referenced to

the solvent peak. Melting points were measured using open-ended capillaries on an Electrothermal melting point apparatus and are uncorrected. High-resolution mass spectrometry (HRMS) was performed by the Mass spec service at St Andrews and Dr Stuart Warriner at the University of Leeds.

Thermal analysis. Thermogravimetric analysis (TGA) was conducted on a PerkinElmer Thermal analysis at the University of Durham with a heating rate of 10 °C/min under nitrogen flow. The samples were heated from 30 °C to 700 °C and the thermal decomposition (T_d) was determined at a 5% weight loss.

Electrochemistry measurements. Cyclic Voltammetry (CV) and Differential pulse voltammetry (DPV) analysis was performed on an Electrochemical Analyzer potentiostat model 620D from CH Instruments. Samples were prepared in dichloromethane (DCM) or dimethylformamide (DMF) solutions, which were degassed by sparging the relevant solvent with saturated nitrogen gas for 5 minutes prior to measurements. All measurements were performed using 0.1 M tetra-*n*-butylammonium hexafluorophosphate, $[nBu_4N]PF_6$, in the relevant solvent. An Ag/Ag^+ electrode was used as the reference electrode, a glassy carbon electrode was used as the working electrode and a platinum electrode was used as the counter electrode. The redox potentials are reported relative to a saturated calomel electrode (SCE) with a ferrocene/ferrocenium (Fc/Fc^+) redox couple as the internal standard (0.46 V vs SCE for DCM, 0.45 V vs SCE for DMF).[1] The HOMO and LUMO energies were determined using the relation $E_{HOMO/LUMO} = -(E_{oxonset} / E_{redonset} + 4.8)$ eV, where $E_{oxonset}$ and $E_{redonset}$ are the onset of anodic and cathodic peak potentials, respectively calculated from DPV relative to Fc/Fc^+.[2]

Photophysical measurements. Optically dilute solutions of concentrations on the order of 10^{-5} or 10^{-6} M were prepared in HPLC grade solvent for absorption and emission analysis. Absorption spectra were recorded at room temperature on a Shimadzu UV-2600 double beam spectrophotometer. Steady-state photoluminescence spectra in solution were recorded at 298 K using Shimadzu FS5 Spectro fluorophotometer and Jasco FP-8600 spectrofluorometer. A Jasco FP-8600 spectrofluorometer with an integrating sphere was employed for quantum yield measurements for thin film samples.[3] Doped thin films were prepared by mixing the sample (1, 3, 5, 7, 10, 15, 20, 100 wt.%) and mCP in chloroform followed by spin-casting on a quartz substrate. The Φ_{PL} of the films were then measured in air and by purging the integrating sphere with N_2 gas flow. Time-resolved PL measurements of the thin films were carried out using an iCCD camera with integration times being ten times shorter than the delays times. The samples were excited at 355 nm by a q-switched laser from QS Lasers (MPL15100-DP). Emission from the samples was focused onto a spectrograph (Oriel MS257) and detected on a gated iCCD camera (iStar A-DH334T-18F-03). The measurements were recorded under vacuum or helium atmosphere unless otherwise stated. Phosphorescence spectra were obtained using a Jasco FP-8600 spectrofluorometer at 77 K, with a delay time of 70 ms for toluene and 20 ms for mCP. Time-resolved decays in other OLED hosts Time-resolved measurements were collected using a spectrograph and a Stanford Computer Optics 4Picos ICCD camera, where samples were excited with a Nd:YAG laser (EKSPLA), 10 Hz, 355 nm.

Quantum chemical calculations. The calculations were performed with the Gaussian 16 revision A03 suite for the density functional theory (DFT)[4] and with the Turbomole/7.4 package for SCS-CC2 calculations. We first optimized the ground state using Spin-component scaling coupled-cluster singles-and-doubles model (SCS-CC2)[5, 6] method considering the cc-pVDZ[7] basis set. Vertical excited states were performed on the ground state optimized structure

using SCS-CC2/cc-PVDZ level of theory and computing the two first singlet (S_1 and S_2[8]) and two first triplet excited states (T_1 – T_2[9]). Excited state optimized S_1 and T_1 states were performed at the DFT level using PBE0[10] within the Tamm-Dancoff approximation (TDA)[11] with the 6-31G(d,p)[12] basis set. SCS-CC2/cc-PVDZ S_1 and T_1 excitation energies are obtained using the TDA-DFT optimized structures. Frequency calculations were implemented using the S_1 and T_1 optimized geometries of **DiCz-*p*-2** at the PBE0/6-31G(d,p) level of theory and using an undistorted displaced harmonic oscillator model to simulate the spectra. The 0-0 transitions was aligned to the value computed from Table **S6** (3.06 eV for S_1; 2.78 eV for T_1). Molecular orbitals were visualized using GaussView 6.0 software.[13] Different density plots were used to visualize change in electronic density between the ground and excited state and were obtained using the VESTA package.[14]

OLED fabrication and testing. Organic light-emitting diodes (OLEDs) were fabricated on patterned indium-tin-oxide (ITO) coated glass (VisionTek Systems) with a sheet resistance of 15 Ω/cm^2 using vacuum thermal evaporation. The substrates were sonicated for 15 minutes each in acetone and then IPA. After oxygen-plasma cleaning, the substrates were loaded into a Kurt J. Lesker Super Spectros 200 deposition chamber. All organic and cathode layers were thermally evaporated at a pressure below 10^{-7} mbar, at evaporation rates in the range of 0.1-0.5 A/s and forming pixels of 2×2, 2×4, and 4×4mm. The materials used for the device fabrication were: N,N'-bis-(naphthalene-1-yl)-N,N'-bis(phenyl)benzidine (NPB, Lumtec), 4,4-(diphenylsilanediyl)bis(N,N-diphenylaniline) (TSBPA, Lumtec), 3,3′-Di(9H-carbazol-9-yl)-1,1′-biphenyl (mCBP, Ossila), 1,3,5-tris(N-phenylbenzimidazol-2-yl)benzene (TPBi, Lumtec), 2,4,6-tris(biphenyl-3-yl)-1,3,5-triazine (T2T, Ossila), bis[2-(diphenylphosphino)phenyl]ether oxide (DPEPO, Sigma Aldrich), lithium fluoride (LiF, Sigma Aldrich), 8-Quinolinolato lithium (Liq, Ossila) and aluminium (Al, Alfa Aesar) which were either purchased from the companies pre-sublimed or sublimation purified before use (Creaphys DSU05). Characterization of OLED devices was conducted in a 10-inch integrating sphere (Labsphere) coupled

with a calibrated fibre spectrometer (Ocean Optics USB4000) and connected to a Keithley 2400 source measure unit.

Literature Study

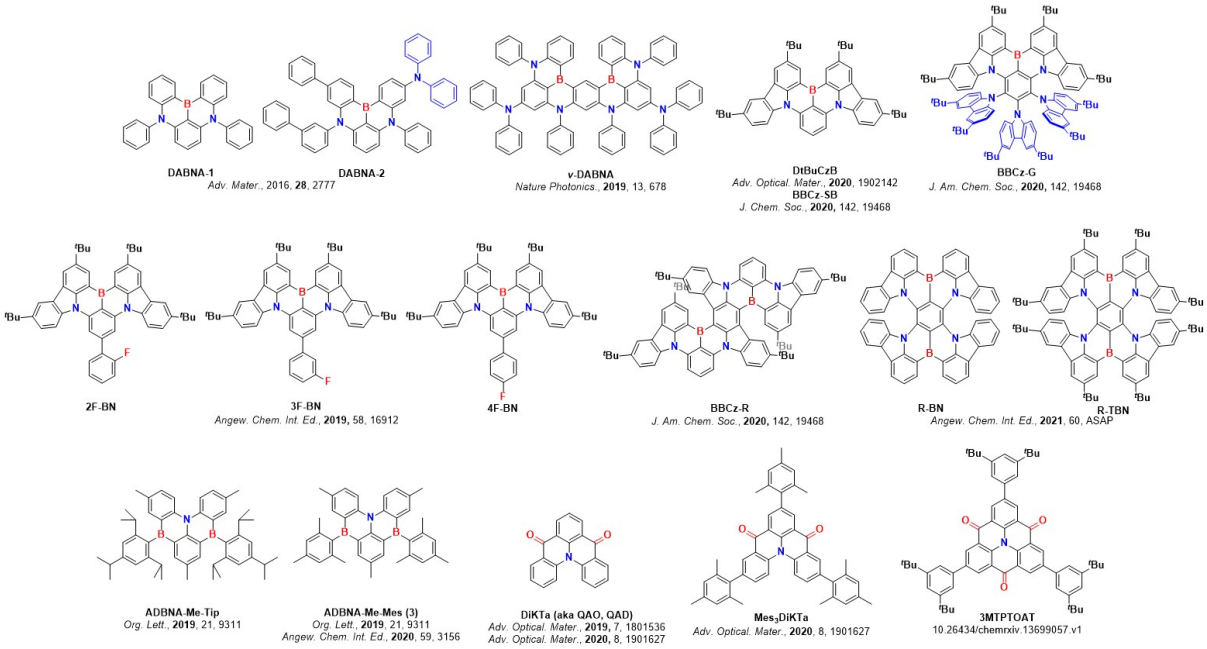

Figure **S1**. Structures of discussed literature MR-TADF emitters.

Table **S1**. Optoelectronic and device properties of high performing MR-TADF emitters

Compound	**Medium**	**λ_{PL} / nm**	**Φ_{PL} / %**	**τ_D / μs**	**ΔE_{ST} / eV**	**λ_{EL} / nm**	**CIE_{XY}**	**EQE_{max} / %**	**EQE_{100} / %**	**Roll-off 1000 cd m^{-2} / %**	**Ref**
DABNA-1	1 wt% mCBP	460	88	94	0.18	459	0.13,0.09	13.5	~6.3	N/A	[15]
DABNA-2	1 wt% mCBP	469	90	65	0.14	467	0.12,0.13	20.2	~13.3	N/A	[15]
***ν*-DABNA**	1 wt% in DOBNA-OAr	467	90	4.1	0.02	469	0.12,0.11	34.4	32.7	26.1	[16]
DtBuCzB	1 wt% mCBP	493	88	69	0.13[a]	488	0.10,0.42	21.6	15.0	5.3	[17, 18]
2F-BN	6 wt% mCBP	502	89	25.6	0.16[a]	501	0.16,0.60	22.0	20.1	15.0	[19]
3F-BN	6 wt% mCBP	503	83	16.7	0.08[a]	499	0.20,0.58	22.7	22.3	21.1	[19]
4F-BN	6 wt% mCBP	501	91	19.0	0.11[a]	493	0.12,0.48	20.9	19.2	16.4	[19]
BBCz-G	2 wt% mCBP	519	99	13	0.14[a]	515	0.26,0.68	31.8	~29.5	~22.3	[18]
BBCz-R	2 wt% mCBP	619	79	53	0.19[a]	616	0.67,0.33	22.0	~5	N/A	[18]
R-BN	3 wt% CBP	672	100	310	0.18[a]	664	0.72,0.28	28.4	N/A	N/A	[20]
R-TBN	3 wt% CBP	698	100	710	0.16[a]	686	0.72,0.28	28.1	N/A	N/A	[20]
ADBNA-Me-Mes	1 wt% in DOBNA-OAr	482	89	165	0.18	480	0.10,0.27	16.2	11.2	N/A	[21, 22]
ADBNA-Me-Tip	1 wt% in DOBNA-OAr	479	88	147	0.18	481	0.11,0.29	21.4	15.4	N/A	[21]
QAO/QAD/DiKTa	5 wt% mCP	466	72	93.3	0.19	468	0.13,0.18	19.4	~9.4	~1.4	[23]
Mes_3DiKTa	3.5 wt% mCP	477	80	20	0.21	480	0.12,0.32	21.1	14.5	4.5	[24]
3MTPTOAT	15 wt% mCP	502	92	N/A	0.14	516	0.21,0.62	31.2	N/A	N/A	[25]

[a]In dilute toluene solution, where ~ indicates data were extracted using graphical fitting software (https://apps.automeris.io/wpd).

Table **S2**. TADF properties of literature MR-TADF emitters.

Emitter	Medium	Φ_p	τ_p / ns	Φ_d	τ_d / μs	ΔE_{ST} / eV	k_{ISC} / × 10^7 s^{-1}	k_{RISC} / × 10^2 s^{-1}	Ref
MCz-TXT	10 wt% mCBP	N/A	N/A	N/A	0.75	0.04	94	1100000	[26]
5Cz-TRZ	Toluene	N/A	5.7	N/A	1.9	0.06	32	150000	[27]
TpAT-tFFO	Toluene	2	15	82	4.4	0.02	5.3	120000	[28]
BSBS-N1	2 wt% mCBP	8	0.9	81	5.6	0.14	100	19000	[29]
m-Cz-BNCz	10 wt% PhCzBCz	85	8.8	11	0.86	0.08	1.3	10800	[30]
v-DABNA	1 wt% DOBNA-OAr	82	4.1	8	4.1	0.02	2.3	2000	[16]
BBCz-G	Toluene	29	5.0	61	17	0.14	14	1800	[18]
ADBNA-Me-Tip	1 wt% DOBNA-OAr	66	6.0	21	147	0.18	4.1	900	[21]
DiKTa	Toluene	25	5.1	1	23	0.19	0.75	460	[24]
4F-BN	6 wt% mCPBC				19	0.11	1.6	440	[19]
3F-BN	6 wt% mCPBC	N/A	N/A	N/A	17	0.08	2.0	390	[19]
Mes3DiKTa	Toluene	36	6.7	1	33	0.21	0.40	310	[24]
2F-BN	6 wt% mCPBC	N/A	N/A	N/A	26	0.16	1.5	220	[19]
DABNA-2	1 wt% mCBP	84	6.0	5	65	0.14	1.1	150	[15]
BBCz-SB	Toluene	65	4.7	33	102	0.13	7.4	140	[18]
BBCz-R	Toluene	65	6.1	24	89	0.19	5.7	120	[18]
DABNA-1	1 wt% mCBP	85	8.8	4	94	0.18	0.45	99	[15]
ADBNA-Me-Mes	1 wt% DOBNA-Oar	71	6.9	18	165	0.18	2.9	76	[31]
R-BN	3 wt% CBP	82	4.7	18	310	0.18	3.9	39	[20]
R-TBN	3 wt% CBP	73	10.3	27	710	0.16	2.6	19	[20]
DiICzMes4	3 wt% mCP	82	12	0.00(1)	438	0.26	1.5	1.8	This work

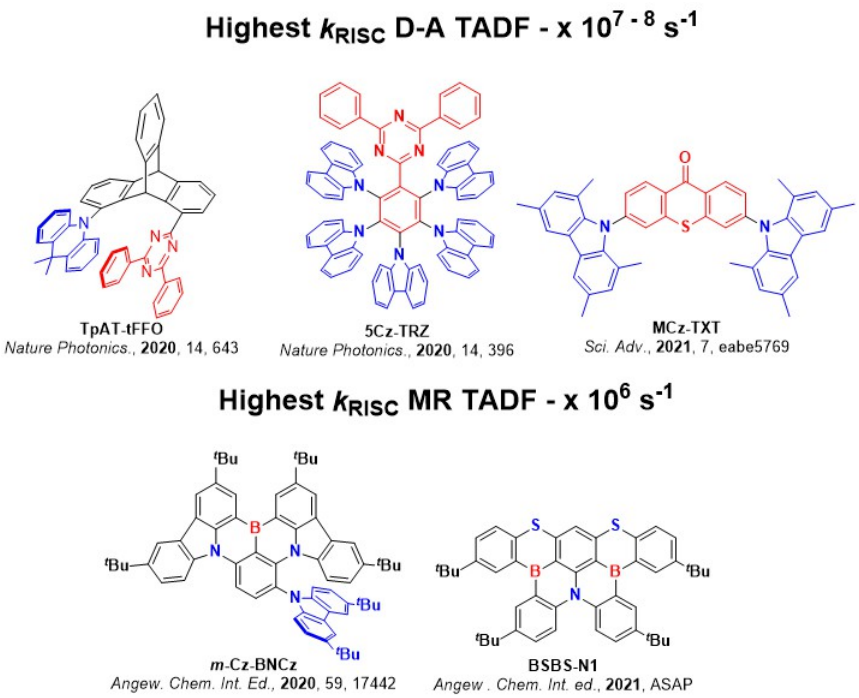

Figure **S2**. Structures of highest k_{RISC} D-A and MR-TADF emitters reported.

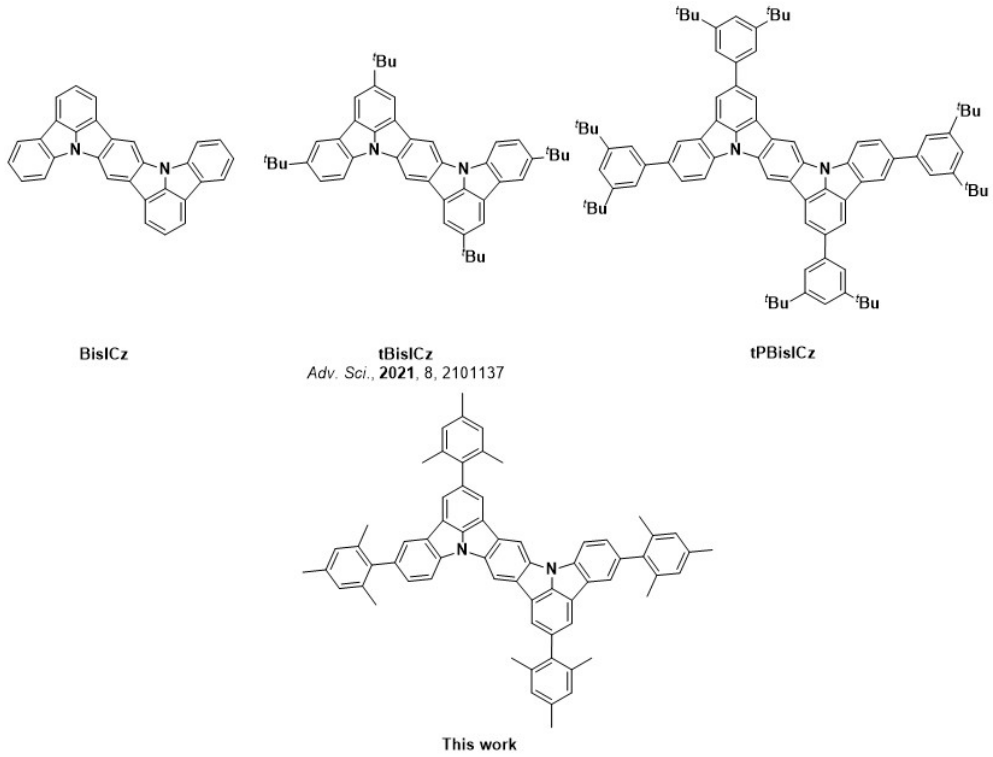

Figure **S3**. Structures of MR-TADF DiIndolocarbazole emitters.

Table **S3**. Summary of conventional OLEDs with DiIndolocarbazole MR-TADF emitters.

	Emitter	V_{on} / V	EQE_{max} / %	EQE_{100} / %	EQE_{1000} / %	Lum_{max} / cd/m^{-2}	CIE (x,y)	λ_{EL} / nm	Ref
Emitter only	**DiICzMes$_4$**	5.2	3.0	1.9	N/A	130	0.15, 0.11	446	This work
	BisICz	3.4[a]	6.5	2.5[a]	N/A	130[a]	0.16, 0.04	437	32
	tBisICz	3.2[a]	15.1	3.0[a]	N/A	200[a]	0.16, 0.05	445	32
	tPBisICz	3.2	23.1	4.8[a]	N/A	230[a]	0.15, 0.05	452	32

[a] Data extracted from graphical fitting software,

Experimental section

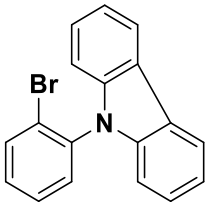

9-(2-bromophenyl)-9H-carbazole - 1

Carbazole (6.69 g, 40.0 mmol, 1.4 equiv.) and oven dried cesium carbonate (13.0 g, 40.0 mmol, 1.4 equiv.) were dried under vacuum for 30 minutes. Dry DMF (80 mL) was added, and the resulting mixture was stirred under N_2 for 30 minutes. 1-bromo-2-fluorobenzene (3.12 mL, 28.6 mmol, 1 equiv.) was added and the resulting mixture was heated to 150 °C for 48 hrs. The reaction was cooled, and water (200 mL) was added. The product was extracted with DCM (3 × 100 mL), dried over Na_2SO_4, filtered and concentrated under reduced pressure to afford the crude product as a off white solid. The crude product was purified by column chromatography on silica gel (5% - 10% DCM:Hexanes). The corresponding fractions were combined and concentrated under reduced pressure to afford a white solid. **Yield:** 96% (8.8 g). **R*f***: 0.37 (10% DCM:Hexanes on silica gel). **Mp**: 92 – 95 °C (Lit Mp: 95 – 96 °C).[33] **^{1}HNMR (500 MHz, CDCl3) δ (ppm)**: 8.16 (d, *J* = 7.8 Hz, 2H), 7.87 (dd, *J* = 8.1, 1.3 Hz, 1H), 7.53 (dd, *J* = 7.4, 1.3 Hz, 1H), 7.49 (dd, *J* = 7.8, 1.8 Hz, 1H), 7.38 – 7.45 (m, 3H), 7.28 – 7.32 (m, 2H), 7.07 (d, *J* = 8.2 Hz, 2H). **^{13}C NMR (126 MHz, $CDCl_3$) δ (ppm)**: 141.0, 136.9, 134.4, 131.3, 130.3, 129.0, 126.1, 124.0, 123.4, 120.5, 120.1, 110.2. The characterization matches that previously reported.[34]

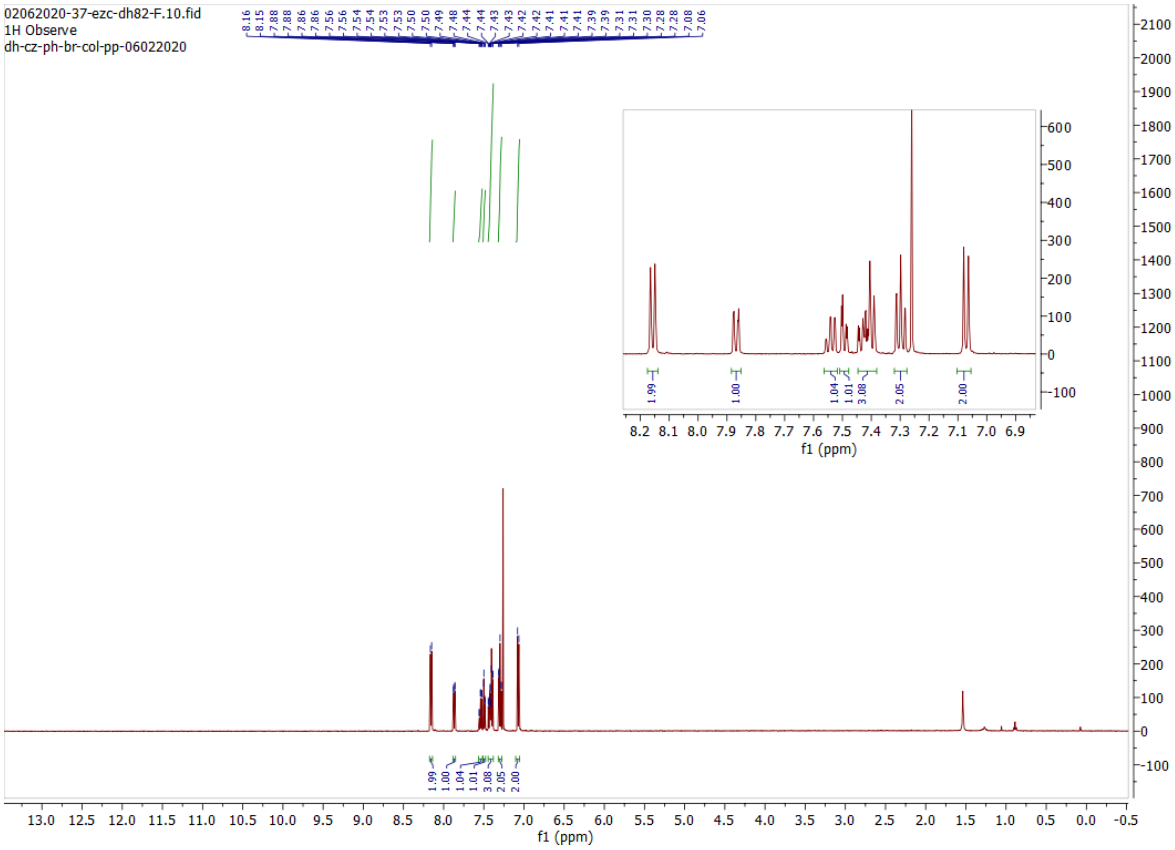

Figure **S4**. ^{1}H NMR of **1** in $CDCl_3$.

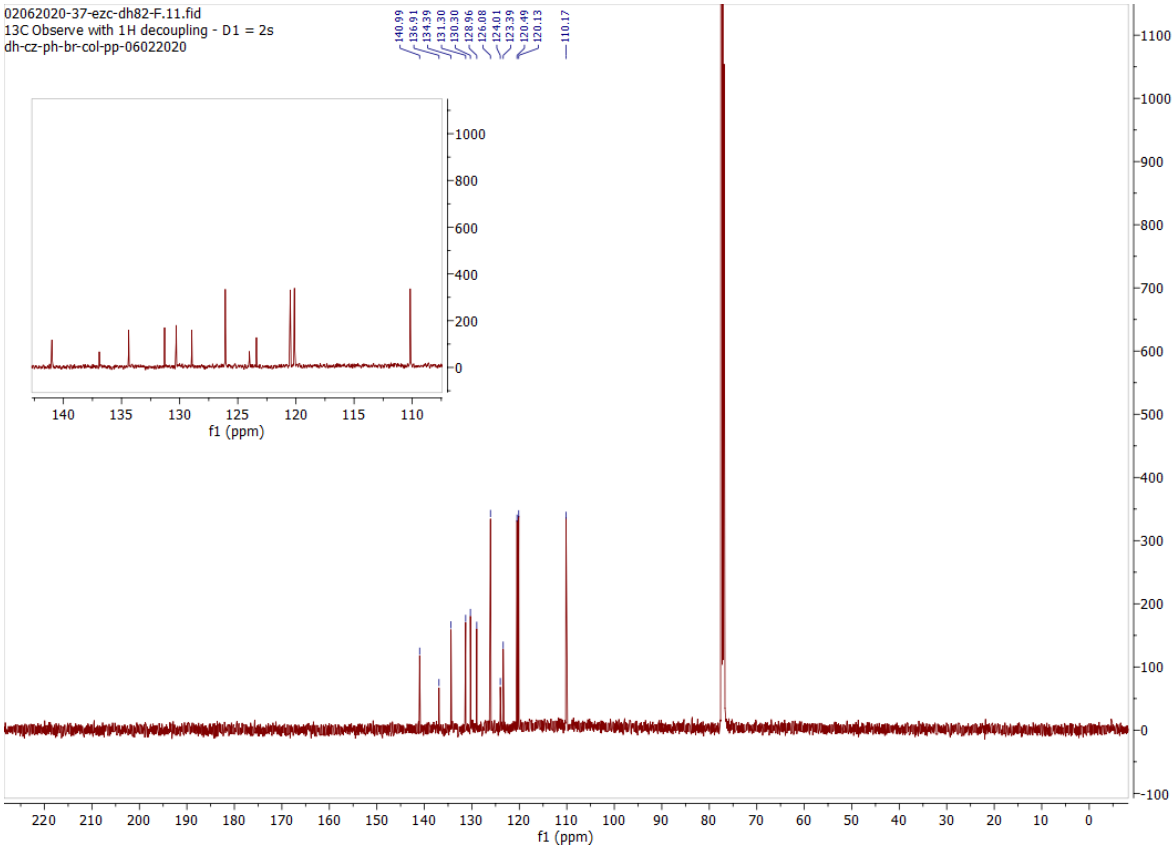

Figure **S5**. ^{13}C NMR of **1** in $CDCl_3$.

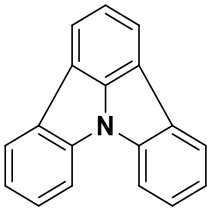

Indolo[3,2,1-jk]-carbazole - ICz

1 (4.00 g, 12.4 mmol, 1 equiv.), K_2CO_3 (8.58 g, 62.1 mmol, 5 equiv.) and tetrabutylammonium bromide (4.00 g, 12.4 mmol, 1 equiv.) were dissolved in *N,N*-Dimethylacetamide (100 mL), the reaction mixture was degassed by bubbling N_2 through for 15 min. $Pd(OAc)_2$ (0.42 g, 1.9 mmol, 0.15 equiv.) and PPh_3 (1.14 g, 4.3 mmol, 0.35 equiv.) were added and the resulting mixture was heated to 160 °C for 48 hours. The reaction mixture was cooled, and water (200 mL) was added, and the product was extracted with DCM (3 × 100 mL), dried over Na_2SO_4, filtered and concentrated under reduced pressure to afford the crude product as a grey solid. The product was purified by column chromatography on silica gel (10% DCM:Hexanes). The corresponding fractions were combined and concentrated under reduced pressure to afford a white solid, which was washed with cold pentane to produce white needle crystals. **Yield:** 85% (2.55 g). **R*f***: 0.26 (10% DCM:Hexanes on silica gel). **Mp**: 129 - 133 °C (lit Mp: 126 – 128 °C).[34] **^{1}HNMR (500 MHz, $CDCl_3$) δ (ppm)**: 8.16 (d, *J* = 8.0 Hz, 2H), 8.06 (d, *J* = 7.5 Hz, 2H), 7.93 (d, *J* = 8.0 Hz, 2H), 7.60 (t, *J* = 7.5 Hz, 1H), 7.57 (td, *J* = 0.9, 7.7 Hz, 2H), 7.37 (td, *J* = 0.9, 7.7 Hz, 2H). **^{13}C NMR (126 MHz, $CDCl_3$) δ (ppm)**: 143.9, 138.9, 130.2, 126.9, 123.3, 123.0, 121.9, 119.6, 118.6, 112.3. 97.6% pure on HPLC analysis, retention time 2.5 minutes in 99% MeOH 1% THF mix. The characterization matches that previously reported.[34]

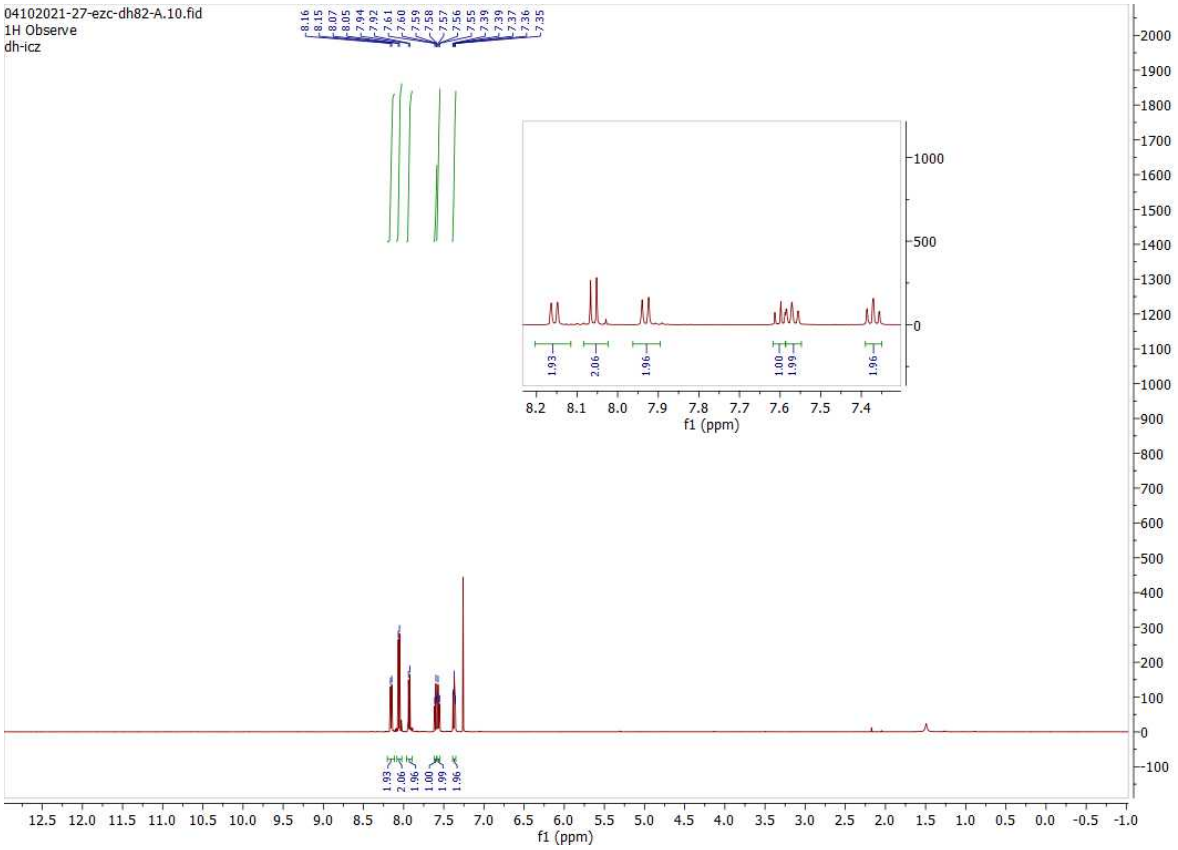

Figure **S6**. ^{1}H NMR of **ICz** in $CDCl_3$.

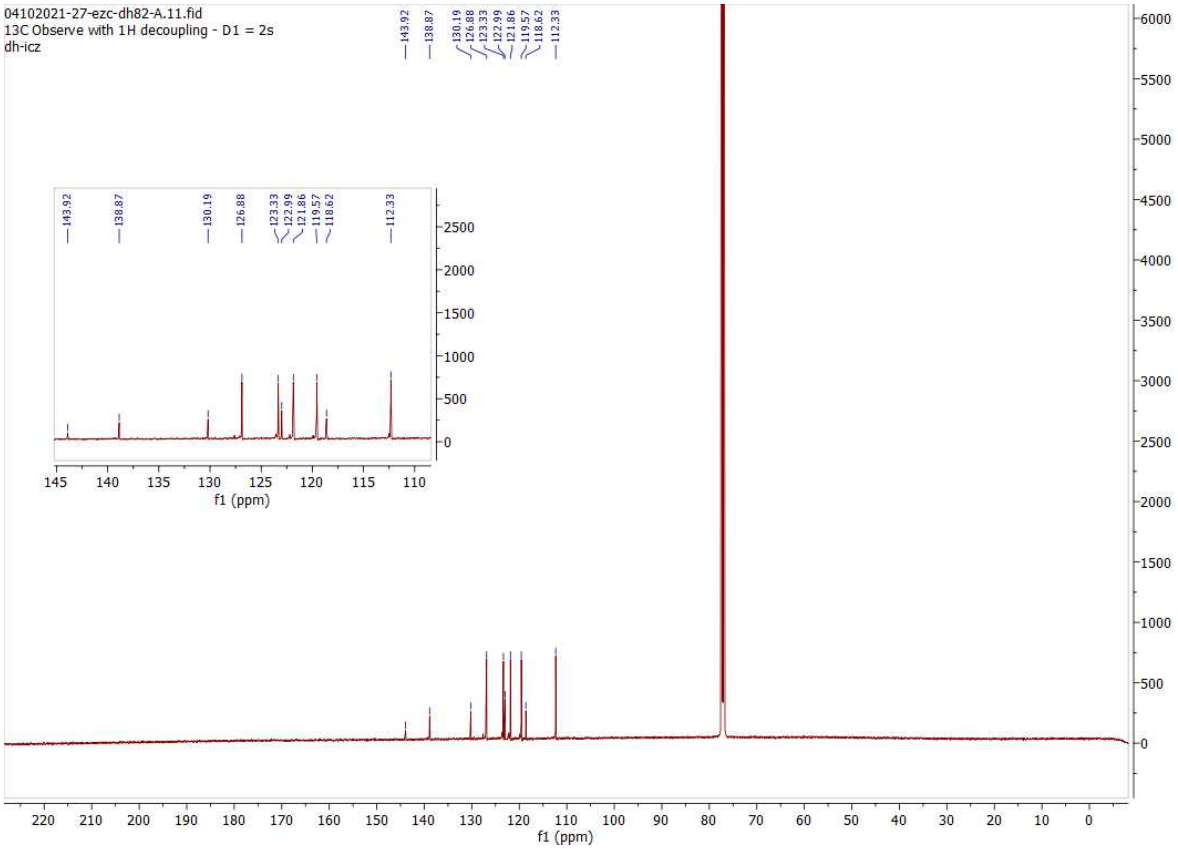

Figure **S7**. ^{13}C NMR of **ICz** in $CDCl_3$.

HPLC Trace Report13Apr2021

<Sample Information>

Sample Name	: icz		
Sample ID	:		
Method Filename	: 99% Methanol 1% THF 20 mins 0.6.lcm		
Batch Filename	: dh-dii-col-p-31032021.lcb		
Vial #	: 1-28	Sample Type	: Unknown
Injection Volume	: 3 uL		
Date Acquired	: 13/04/2021 16:43:36	Acquired by	: System Administrator
Date Processed	: 13/04/2021 17:03:38	Processed by	: System Administrator

<Chromatogram>

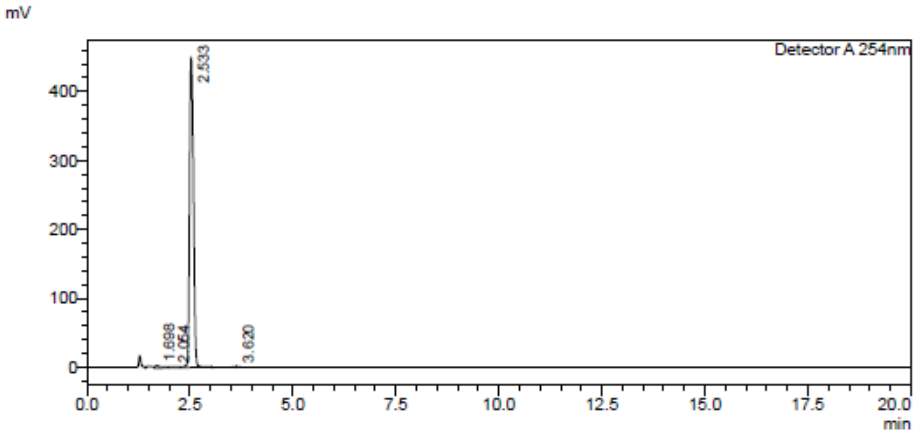

<Peak Table>

Detector A 254nm

Peak#	Ret. Time	Area	Height	Area%	Area/Height	Width at 5% Height
1	1.698	44149	3446	1.434	12.810	--
2	2.054	22579	1541	0.733	14.654	--
3	2.533	3006565	448294	97.634	6.707	0.198
4	3.620	6126	779	0.199	7.866	0.244
Total		3079419	454060	100.000		

Figure **S8**. HPLC trace of **ICz**.

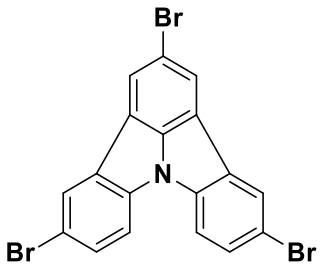

2,5,11-tribromoindolo[3,2,1-jk]carbazole – ICzBr$_3$

ICz (1.50 g, 6.2 mmol, 1 equiv.) was added to dry DMF (30 mL). *N*-Bromosuccinimide (3.65 g, 20.5 mmol, 3.3 equiv.) was added in portions and the resulting mixture was stirred at room temperature in darkness for 24 hours. Saturated sodium thiosulfate (50 mL) was added, and the resulting reaction mixture was extracted with DCM (5 × 100 mL) and concentrated under reduced pressure. The reaction

mixture was sonicated in EtOAc (100 mL), filtered and dried to afford the compound as a white solid. **Yield:** 79% (2.35 g). **Mp**: 297 - 301 °C. **^{1}HNMR (500 MHz, DMSO-d$_6$) δ (ppm)**: 8.57 (d, J = 2.0 Hz, 2H), 8.49 (s, 2H), 8.29 (d, J = 8.6 Hz, 2H), 7.81 (dd, J = 8.6, 2.0 Hz, 2H). **^{13}C NMR (126 MHz, DMSO-d$_6$) δ (ppm)**: 141.9, 137.1, 130.5, 130.2, 126.8, 124.1, 118.5, 115.7, 114.9. The characterization matches that previously reported.[35]

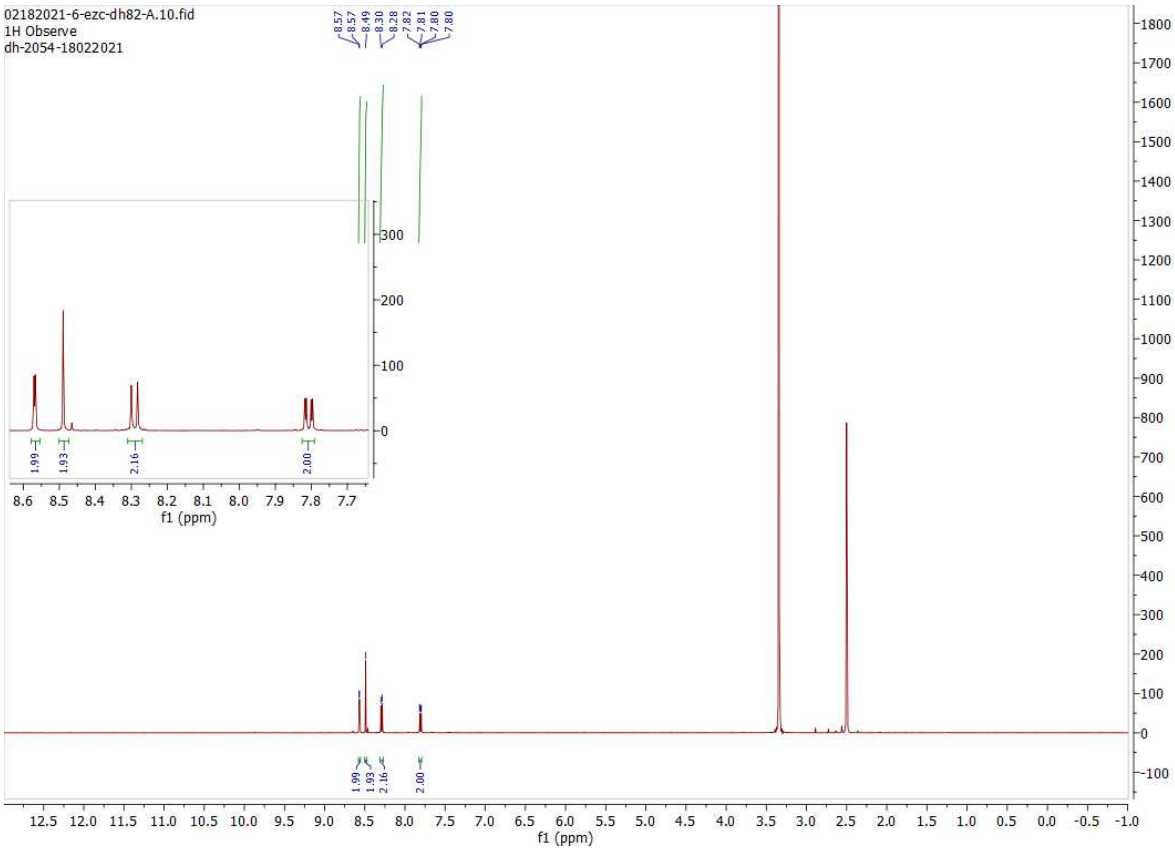

Figure **S9**. ^{1}H NMR of **ICzBr$_3$** in DMSO-d$_6$.

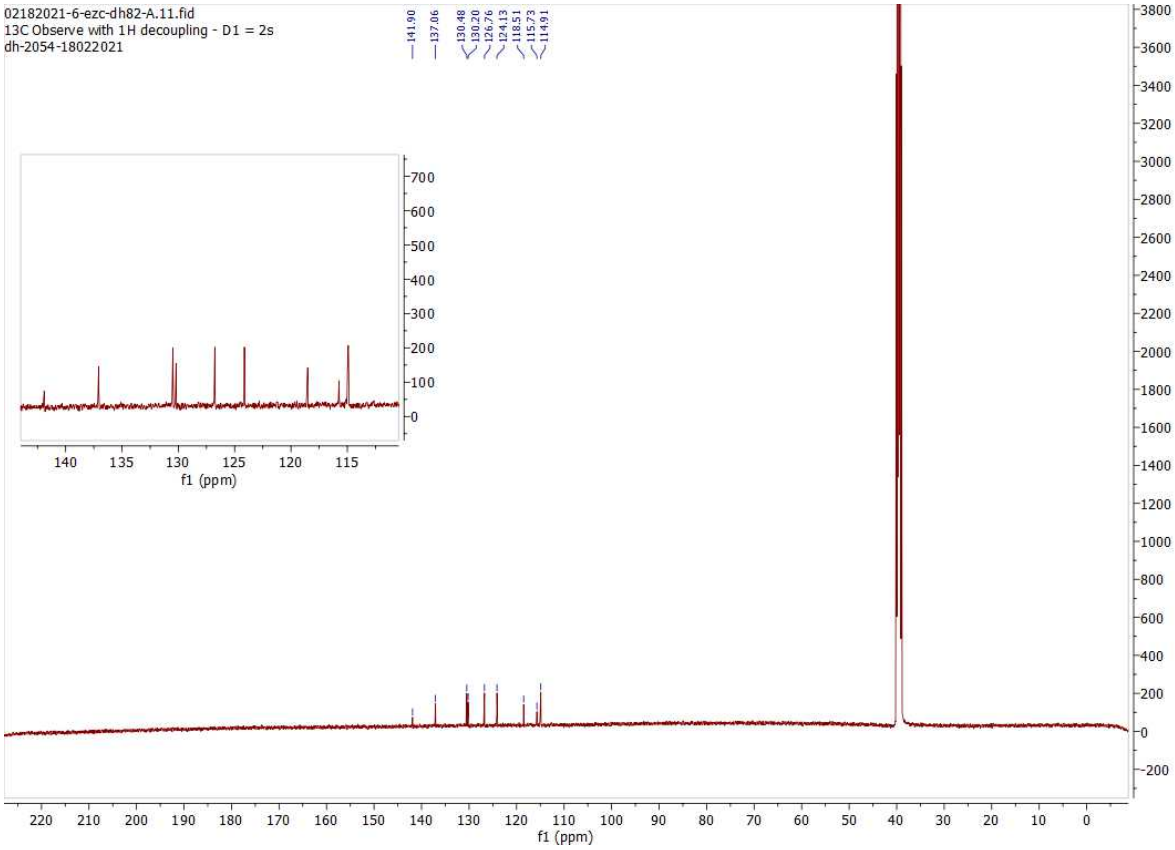

Figure **S10**. ^{13}C NMR of **ICzBr$_3$** in DMSO-d$_6$.

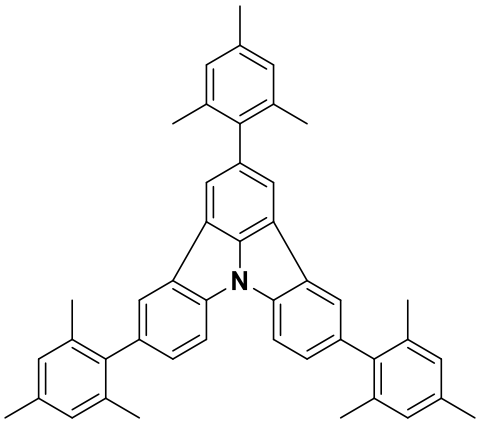

2,5,11-trimesitylindolo[3,2,1-jk]carbazole – ICzMes$_3$

Cesium carbonate (2.39 g, 7.32 mmol, 7 equiv.), **ICzBr$_3$** (0.50 g, 1.05 mmol, 1 equiv.) and mesitylboronic acid (1.03 g, 6.28 mmol, 6 equiv.) were added to a mixture of toluene (3.75 mL), water (2.50 mL) and ethanol (2.50 mL). The resulting solution was degassed with N_2 bubbling for 30 min.

$Pd(PPh_3)_4$ (0.04 g, 0.04 mmol, 0.03 equiv.) was added and the resulting solution was heated to 100 °C for 24 h. The reaction mixture was cooled, and the product was extracted with EtOAc (3 × 50 mL), dried over Na_2SO_4, filtered and concentrated under reduced pressure to afford crude product as a black solid. The product was purified by column chromatography on silica gel (5% DCM:Hexanes). The corresponding fractions were combined and concentrated under reduced pressure to afford a white solid. **Yield:** 69% (0.43 g). **R*f***: 0.23 (5% DCM:Hexanes on silica gel). **Mp**: 252 - 255 °C. **^{1}HNMR (500 MHz, $CDCl_3$) δ (ppm)**: 8.01 (d, *J* = 8.2 Hz, 2H), 7.88 (d, *J* = 1.3 Hz, 2H), 7.77 (s, 2H), 7.36 (dd, *J* = 8.2, 1.5 Hz, 2H), 7.01 (s, 6H), 2.37 (s, 9H), 2.10 (s, 12H), 2.06 (s, 6H). **^{13}C NMR (126 MHz, $CDCl_3$) δ (ppm)**: 139.1, 137.8, 136.8, 136.7, 136.5, 134.7, 130.3, 128.1(3), 128.0(7), 128.0(6), 124.0, 120.6, 118.6, 112.1, 21.2, 21.1, 21.0. **HR-MS [M+H]$^+$** Calculated: ($C_{45}H_{41}NH$) 596.3312; Found: 596.3302. 99.7% pure on HPLC analysis, retention time 10.1 minutes in 99% MeOH 1% THF mix.

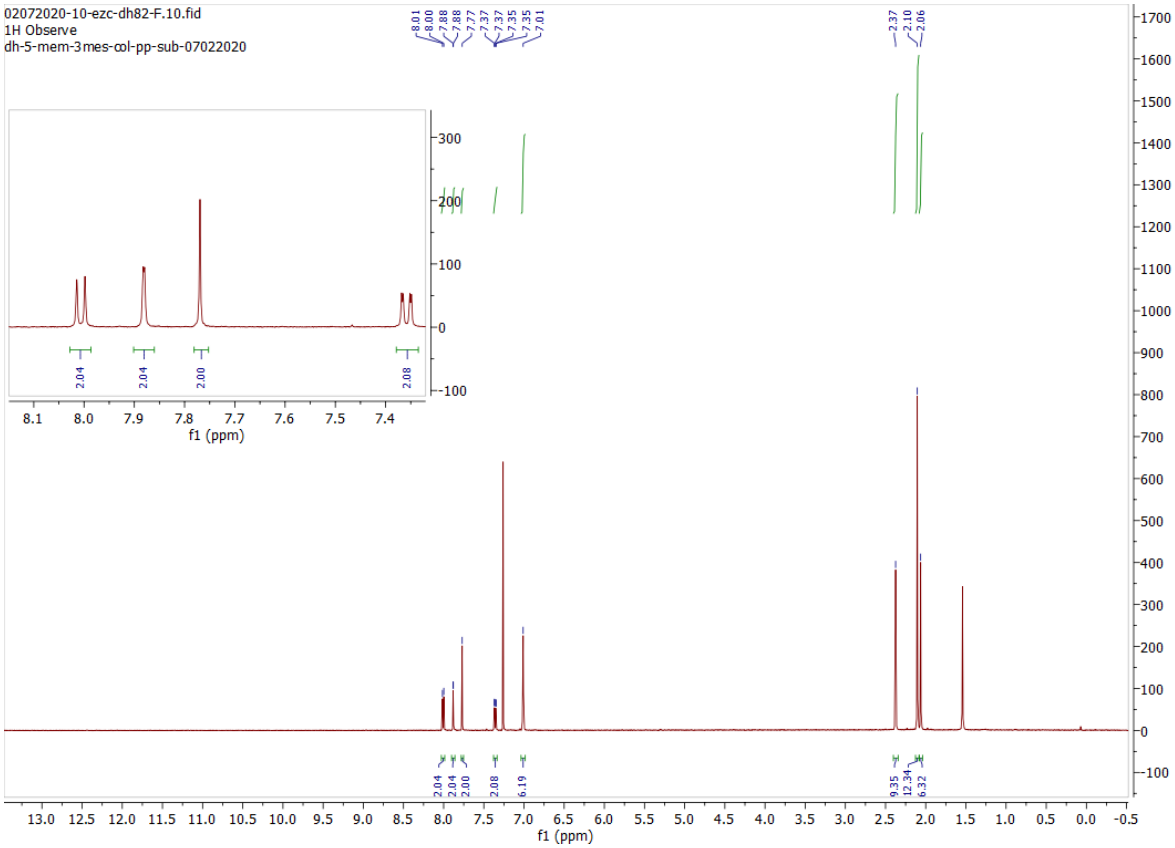

Figure **S11**. ^{1}H NMR of **ICzMes$_3$** in $CDCl_3$.

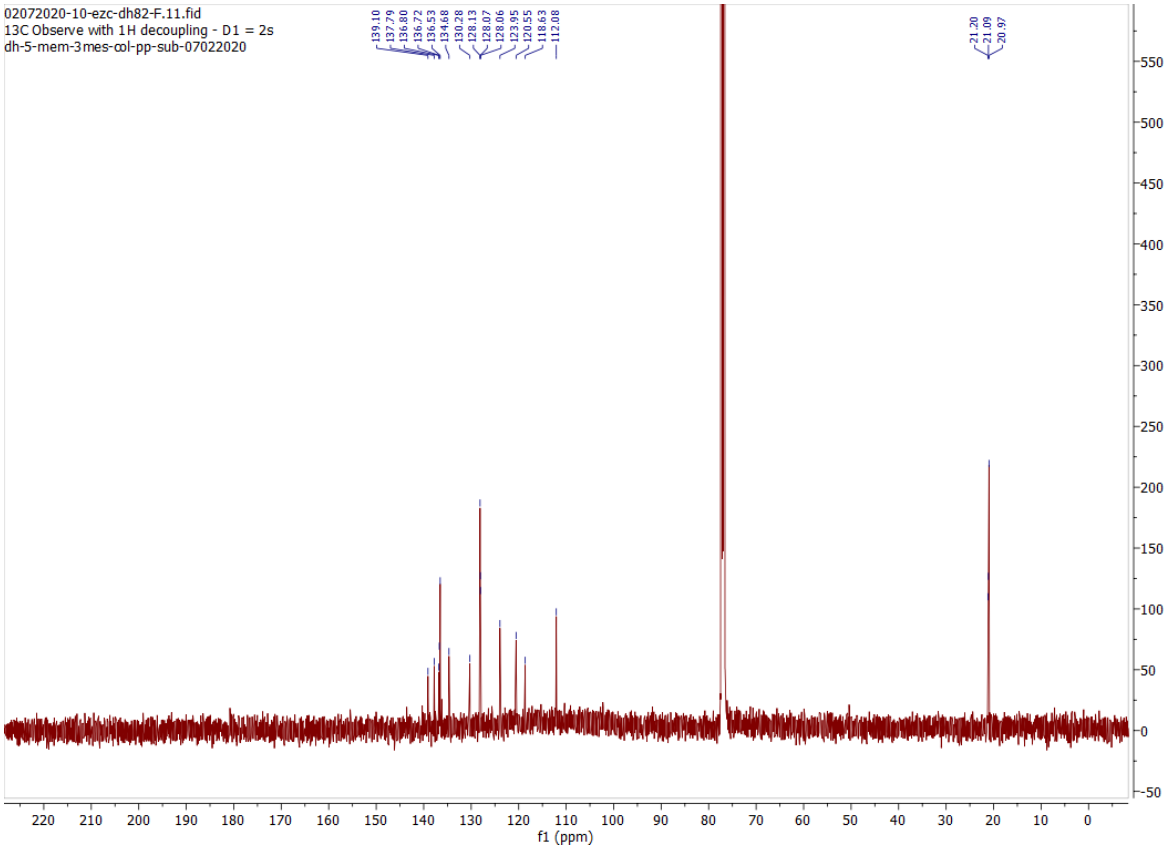

Figure **S12**. ^{13}C NMR of **ICzMes$_3$** in $CDCl_3$.

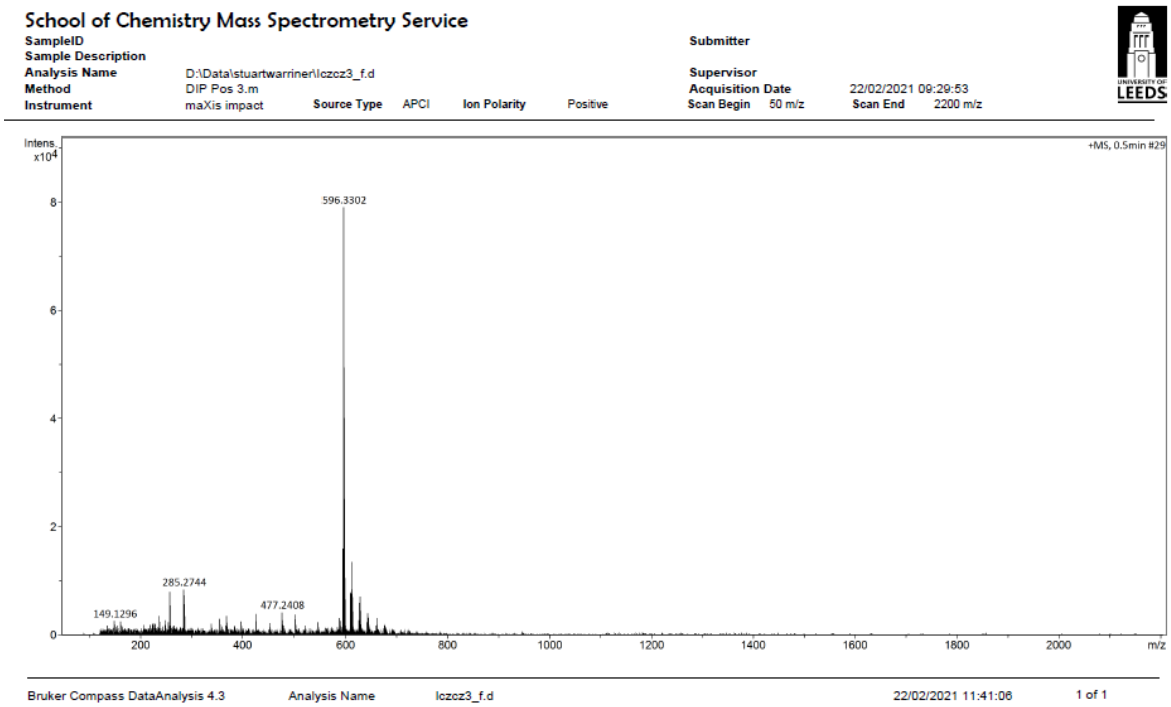

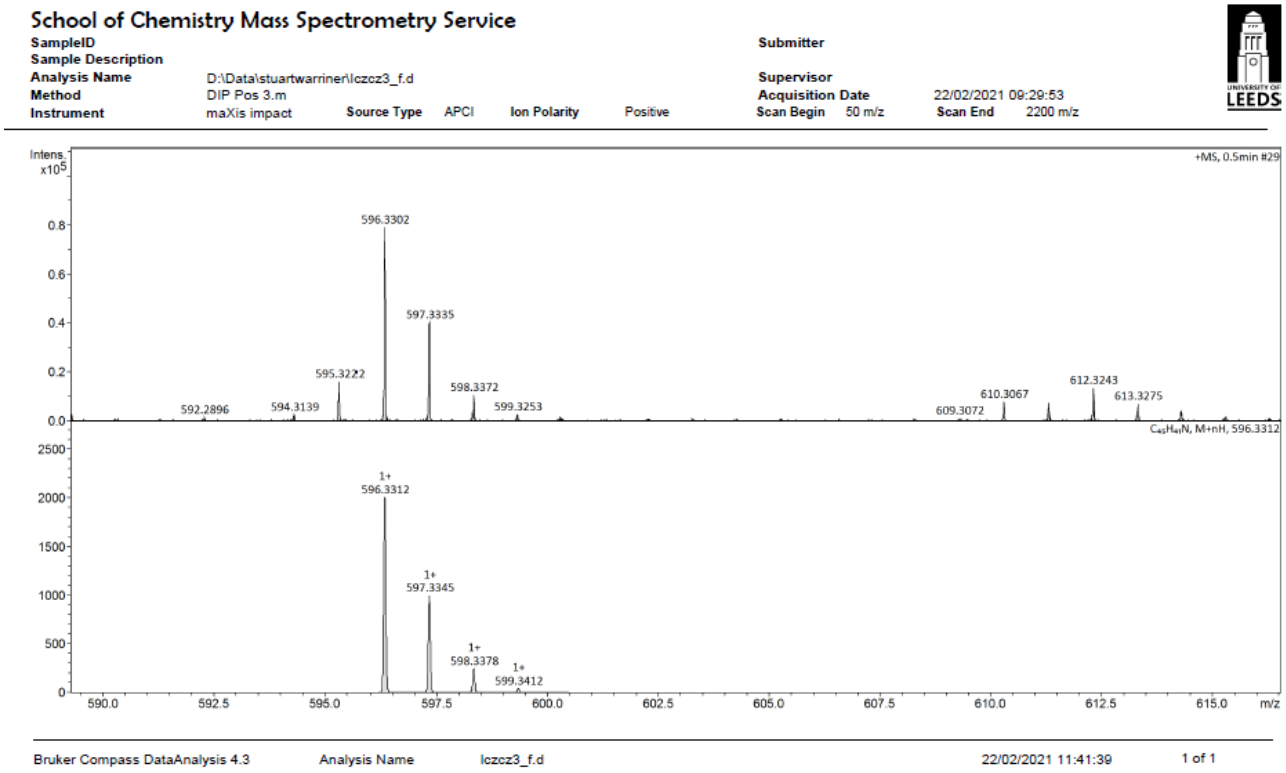

Figure **S13**. HRMS of **ICzBr$_3$**.

HPLC Trace Report27Jan2021

<Sample Information>

Sample Name	: icz-mes3		
Sample ID	:		
Method Filename	: 99% Methanol 1% THF 20 mins.lcm		
Batch Filename	: icz-mes3-post-sub-27012021-thf.lcb		
Vial #	: 2-2	Sample Type	: Unknown
Injection Volume	: 5 uL		
Date Acquired	: 27/01/2021 17:59:44	Acquired by	: System Administrator
Date Processed	: 27/01/2021 18:19:45	Processed by	: System Administrator

<Chromatogram>

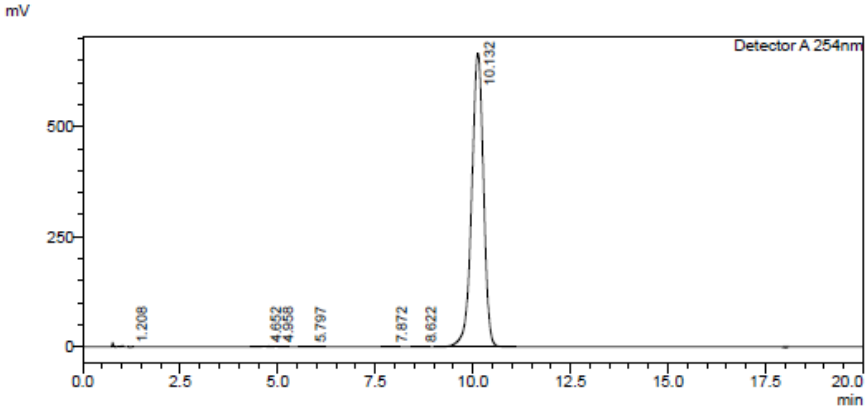

<Peak Table>

Detector A 254nm

Peak#	Ret. Time	Area	Height	Area%	Area/Height	Width at 5% Height
1	1.208	1368	257	0.010	5.328	--
2	4.652	15777	1438	0.112	10.970	--
3	4.958	13145	1183	0.093	11.112	--
4	5.797	2879	143	0.020	20.134	0.608
5	7.872	1613	117	0.011	13.780	0.383
6	8.622	1121	75	0.008	14.910	0.402
7	10.132	14030797	665746	99.745	21.075	0.721
Total		14066700	668960	100.000		

Figure **S14**. HPLC trace report of **ICzMes$_3$**.

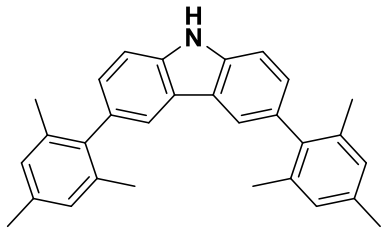

3,6-dimesityl-9H-carbazole - Mes$_2$Cz

The reaction is based on a previously reported synthesis.[36]

Cesium carbonate (35.1 g, 108 mmol, 7 equiv.), 3,6-dibromo-9H-carbazole (5.00 g, 15.4 mmol, 1 equiv.) and mesitylboronic acid (10.1 g, 61.5 mmol, 4 equiv.) were added to a mixture of toluene (56.3 mL), water (37.5 mL) and ethanol (37.5 mL). The resulting solution was degassed with N_2 bubbling for 30 min. $Pd(PPh_3)_4$, (0.53 g, 0.46 mmol, 0.03 equiv.) was added and the resulting solution was heated to

100 °C for 24 hours. The reaction was cooled and extracted with EtOAc (3 × 100 mL), dried over Na_2SO_4, filtered and concentrated under reduced pressure to give an orange oil. The product was purified by column chromatography on silica gel (30% DCM:Hexanes). The corresponding fractions were combined and concentrated under reduced pressure to afford a white solid. The product was recrystalised by slow evaporation from tetrahydrofuran to afford a white crystalline solid. **Yield:** 62% (3.86 g). **R*f***: 0.35 (30% DCM:Hexanes on silica gel). **Mp**: 147 - 151 °C. **^{1}HNMR (500 MHz, CDCl3) δ (ppm)**: 8.14 (s, 1H), 7.78 (d, *J* = 1.3 Hz, 2H), 7.50 (d, *J* = 8.2 Hz, 2H), 7.19 (dd, *J* = 8.22, 1.4 Hz, 2H), 6.98 (s, 4H), 2.36 (s, 6H), 2.06 (s, 12H). **^{13}C NMR (126 MHz, $CDCl_3$) δ (ppm)**: 139.8, 138.7, 136.8, 136.5, 132.4, 128.2, 127.5, 123.6, 120.9, 110.7, 21.2(0), 21.1(7). Spectra in agreement with previously reported.[36]

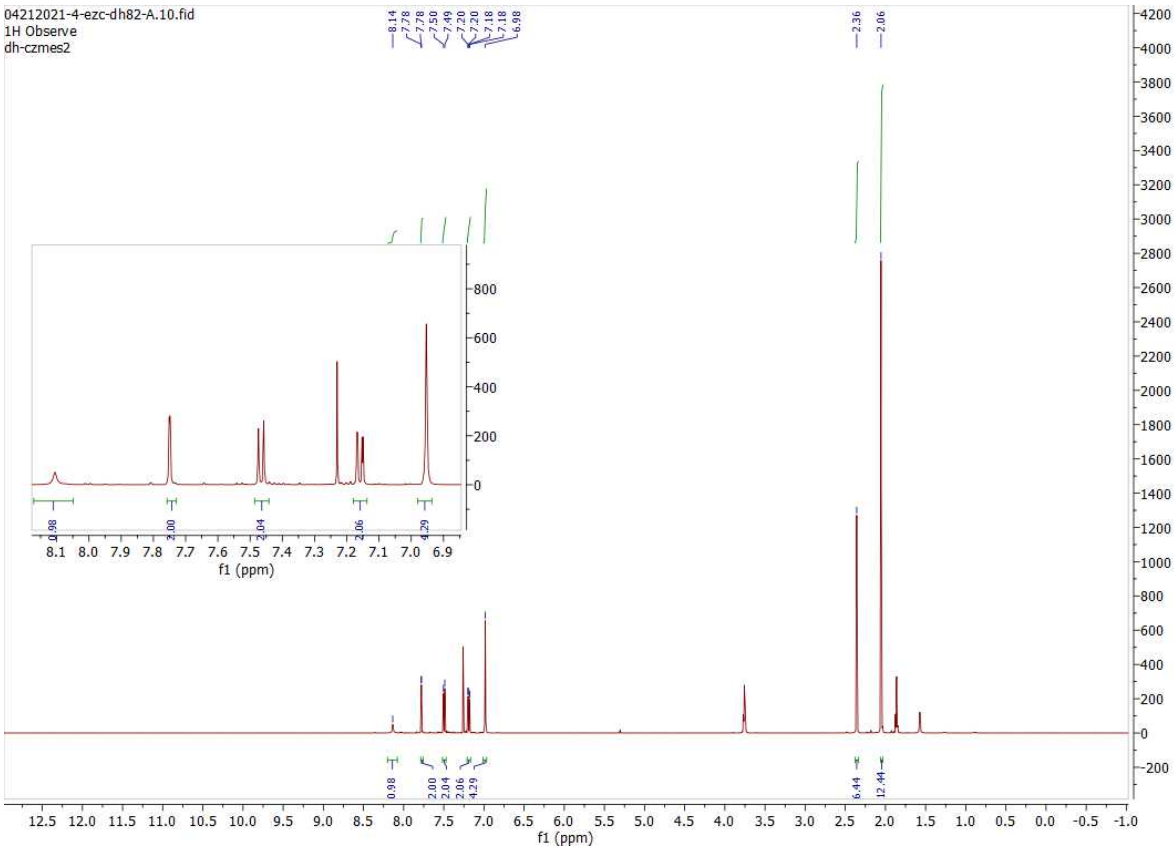

Figure **S15**. ^{1}H NMR of **Mes$_2$Cz** in $CDCl_3$.

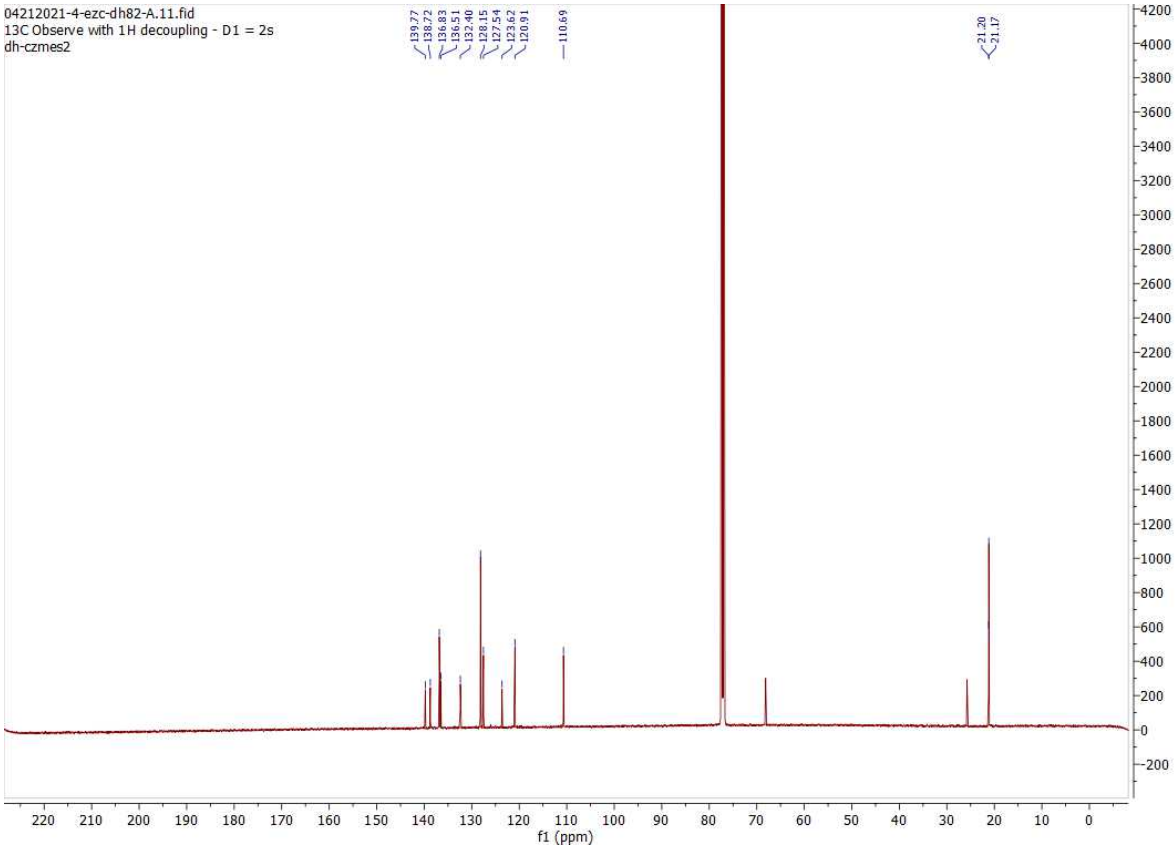

Figure **S16**. ^{13}C NMR of **Mes$_2$Cz** in $CDCl_3$.

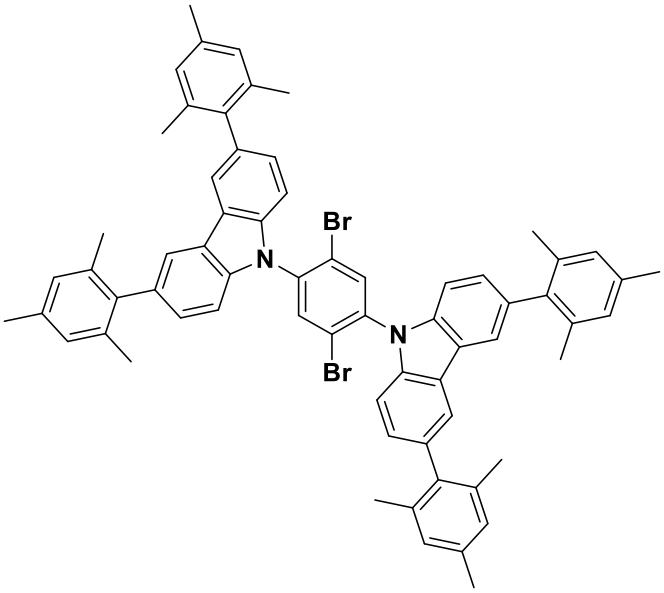

9,9'-(2,5-dibromo-1,4-phenylene)bis(3,6-dimesityl-9H-carbazole) - 2

NaH (60% dispersed in mineral oil, 0.04 g, 1.6 mmol, 2.5 equiv.) was added to dry DMF (12 mL). It was stirred under N_2 and cooled to 0 °C, **Mes$_2$Cz** (0.65 g, 1.6 mmol, 2.5 equiv.) was added in portions and stirred for 30 min. 1,4-dibromo, 2,5-difluorobenzene (0.18 g, 0.64 mmol, 1 equiv.) was added and

the resulting mixture was stirred and heated to 50 °C for 48 h under a N_2 atmosphere. The reaction mixture was cooled and water (30 mL) was added. The product was extracted with DCM (3 × 50 mL), dried over Na_2SO_4, filtered and concentrated under reduced pressure to afford the product as an off-white solid. The product was purified by column chromatography on silica gel (10% - 20% DCM:Hexanes). The corresponding fractions were combined and concentrated under reduced pressure to afford a white solid. The product was recrystalized in a toluene methanol mix (1:1) to afford a white powder. **Yield:** 75% (0.50 g). **R*f***: 0.32 (15% DCM:Hexanes on silica gel). **Mp**: 279 - 283 °C. **^{1}HNMR (500 MHz, $CDCl_3$) δ (ppm)**: 8.15 (s, 2H), 7.88 (d, *J* = 1.1 Hz, 4H), 7.34 (d, *J* = 8.3 Hz, 4 H), 7.28 (d, *J* = 1.1 Hz, 4H), 7.01 (s, 8H), 2.37 (s, 12H), 2.11 (s, 12H), 2.10 (s, 12H). **^{13}C NMR (126 MHz, $CDCl_3$) δ (ppm)**: 139.8, 139.5, 138.6, 136.9, 136.8, 136.1, 133.7, 128.3, 128.0, 123.9, 123.2, 121.2, 110.3, 21.3, 21.2. **HR-MS [M+H]$^+$** Calculated: ($C_{66}H_{58}N_2Br_2H$) 1039.3029; Found: 1039.2990.

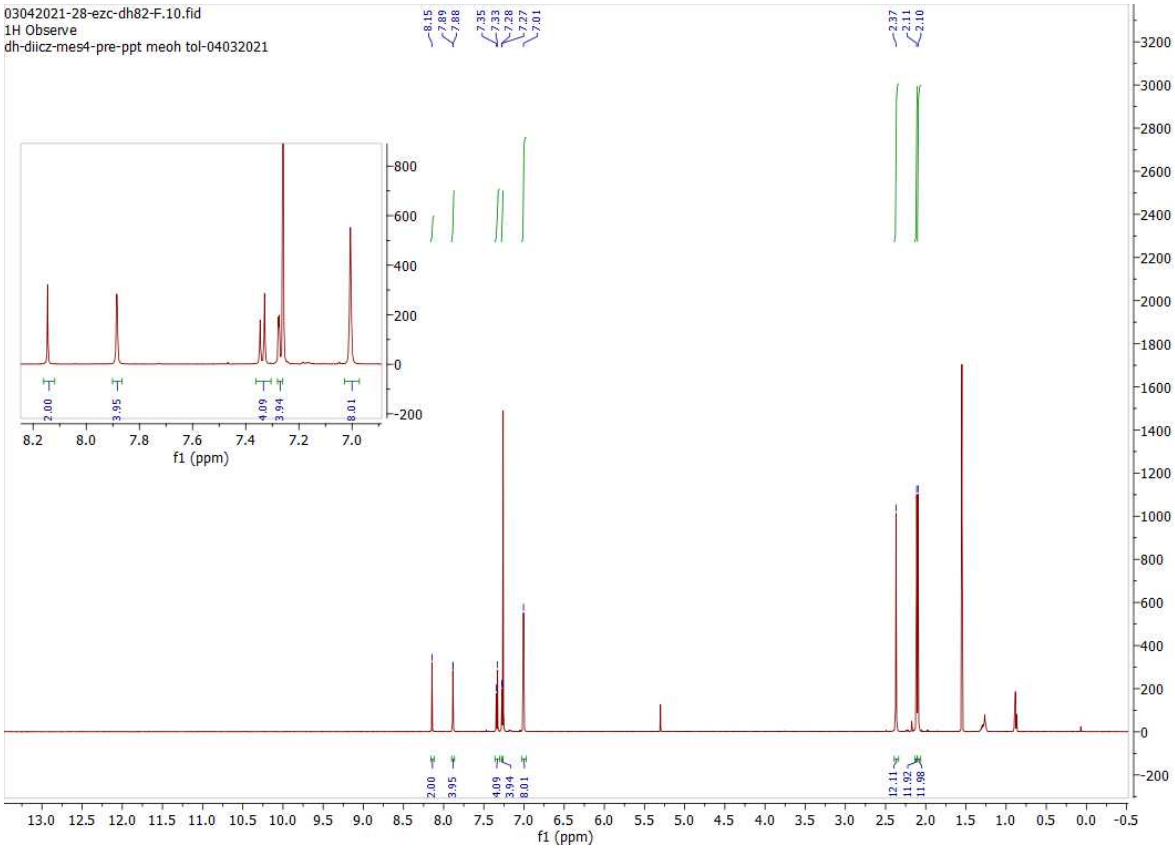

Figure **S17**. ^{1}H NMR of **2** in $CDCl_3$.

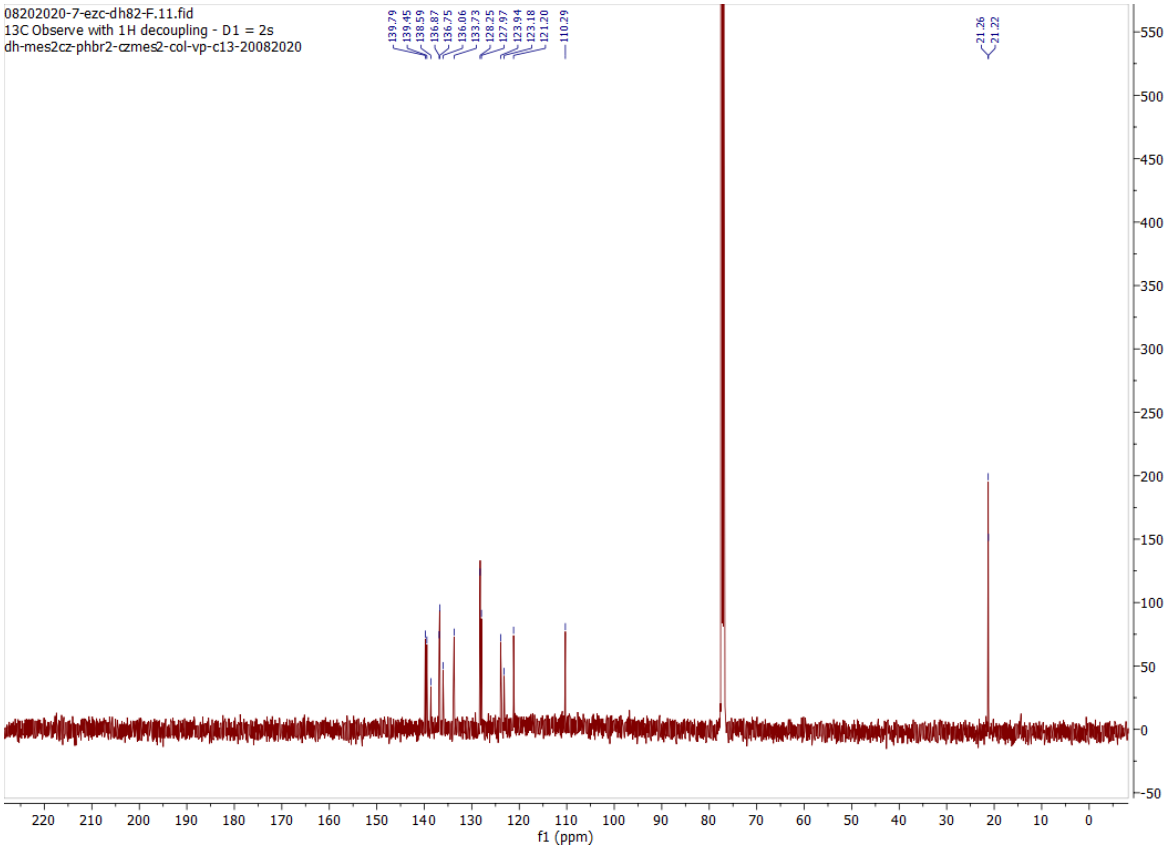

Figure **S18**. ^{13}C NMR of **2** in $CDCl_3$.

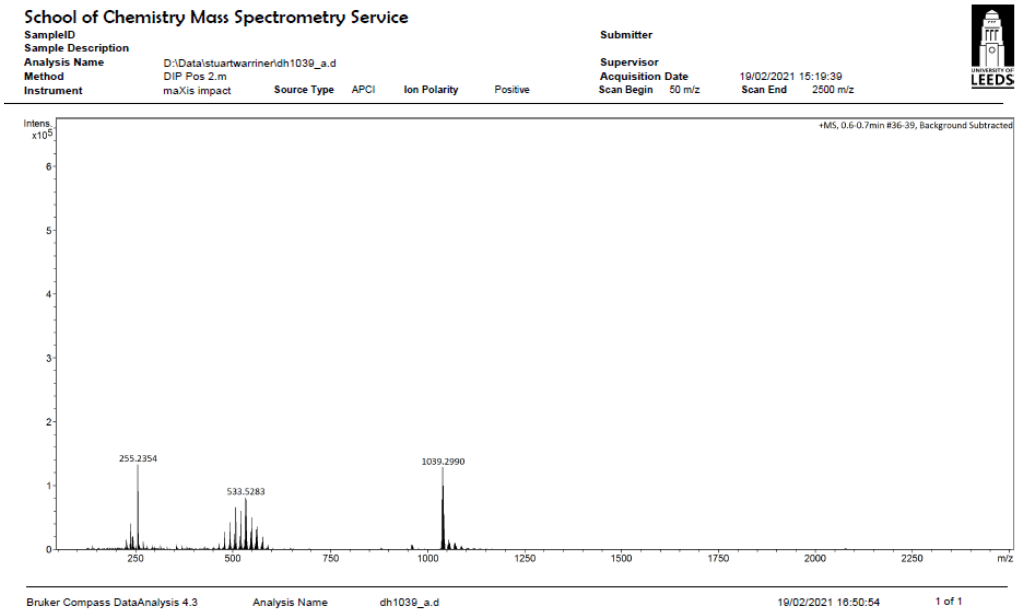

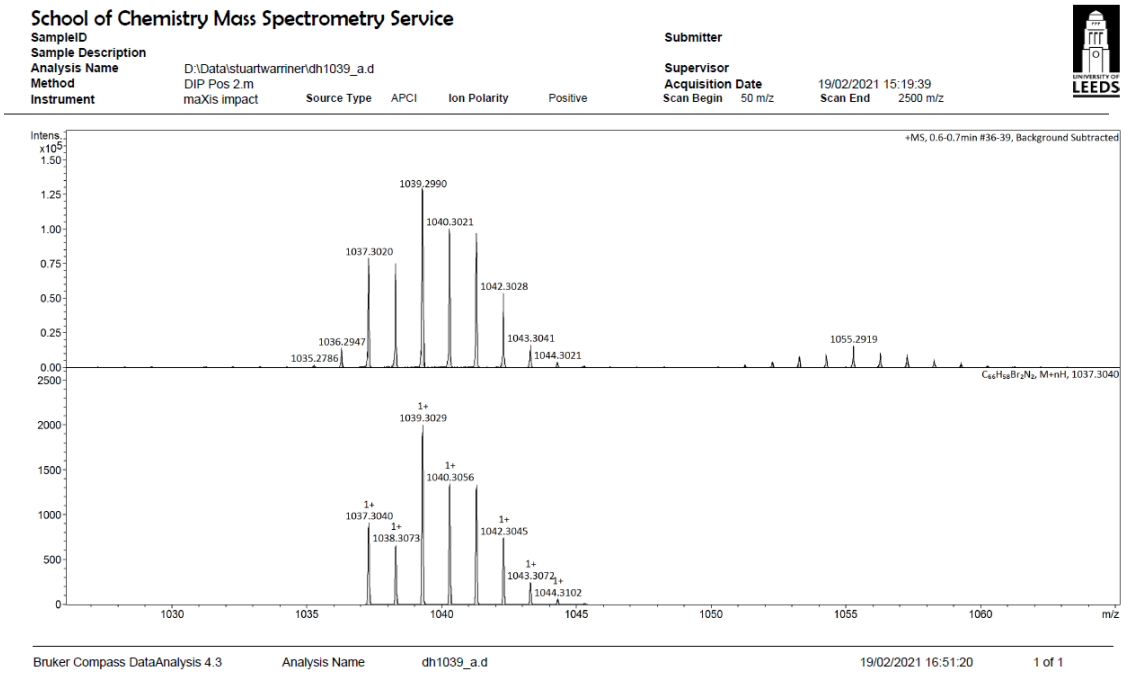

Figure **S19**. HRMS of **2**.

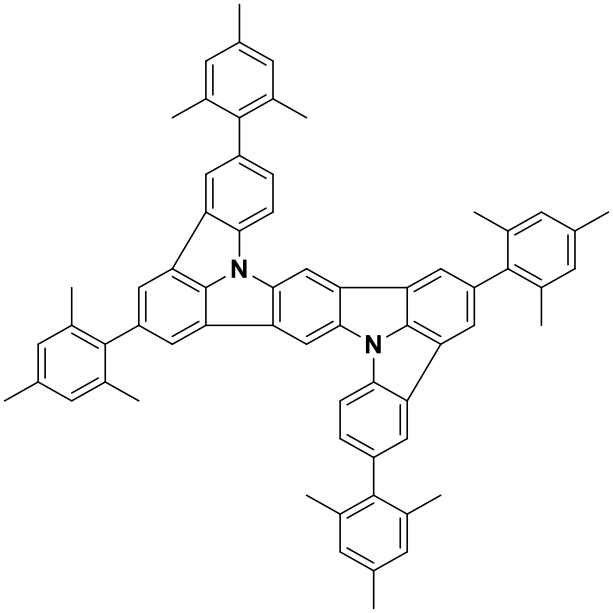

DiICzMes$_4$

2 (0.40 g, 0.4 mmol, 1 equiv.), tetra-*butyl*-ammonium bromide (0.25 g, 0.8 mmol, 2 equiv.), K_2CO_3 (0.53 g, 3.8 mmol, 10 equiv.) were dissolved in *N,N*-Dimethylacetamide (4 mL), the reaction was degassed by bubbling N_2 through the solution for 15 min. $Pd(OAc)_2$ (0.04 g, 0.02 mmol, 0.5 equiv.) and PPh_3 (0.10 g, 0.4 mmol, 1 equiv.) were added and the mixture was heated to 160 °C for 48 h. The reaction was cooled, water (20 mL) was added and the product was extracted with DCM (4 × 50 mL). The organic phase was dried over Na_2SO_4, filtered, and concentrated under reduced pressure to afford the crude product as a black solid. The product was purified by column chromatography on silica gel (5% - 10% DCM:Hexanes). The corresponding fractions were combined and concentrated under reduced pressure to afford a yellow solid. The product was subsequently sonicated in methanol and filtered producing a yellow solid, 0.27 g (80%), which was recrystalized in a toluene methanol mixture (1:1) and filtered to afford pale yellow crystals. **Yield:** 59% (0.20 g). **R*f***: 0.27 (10% DCM:Hexanes on silica gel). **Decomposed**: 392 °C. **^{1}HNMR (500 MHz, $CDCl_3$) δ (ppm)**: 8.67 (s, 2H), 8.15 (d, *J* = 8.2 Hz, 2H), 8.00 (s, 2H), 7.92 (d, *J* = 1.3 Hz, 2H), 7.83 (s, 2H), 7.42 (dd, *J* = 8.2, 1.3 Hz, 2H), 7.06 (s, 4H), 7.02 (s, 4H), 2.42 (s, 6H), 2.38 (s, 6H), 2.12 (s, 24H). **^{13}C NMR (126 MHz, $CDCl_3$) δ (ppm)**: 144.3, 140.4, 139.2, 138.0, 137.0, 136.9, 136.8, 136.7, 136.3, 135.3, 134.7, 130.2, 129.6, 128.3(2), 128.2(8), 128.2(6), 124.1, 120.9, 120.5, 119.0, 118.8, 112.2, 106.8, 21.4, 21.3, 21.2, 21.1. **HR-MS [M]$^+$**

Calculated: ($C_{66}H_{56}N_2$) 876.4443; Found: 876.4418. 99.2% pure on HPLC analysis, retention time 9.1 minutes in 85% MeOH 15% THF mix.

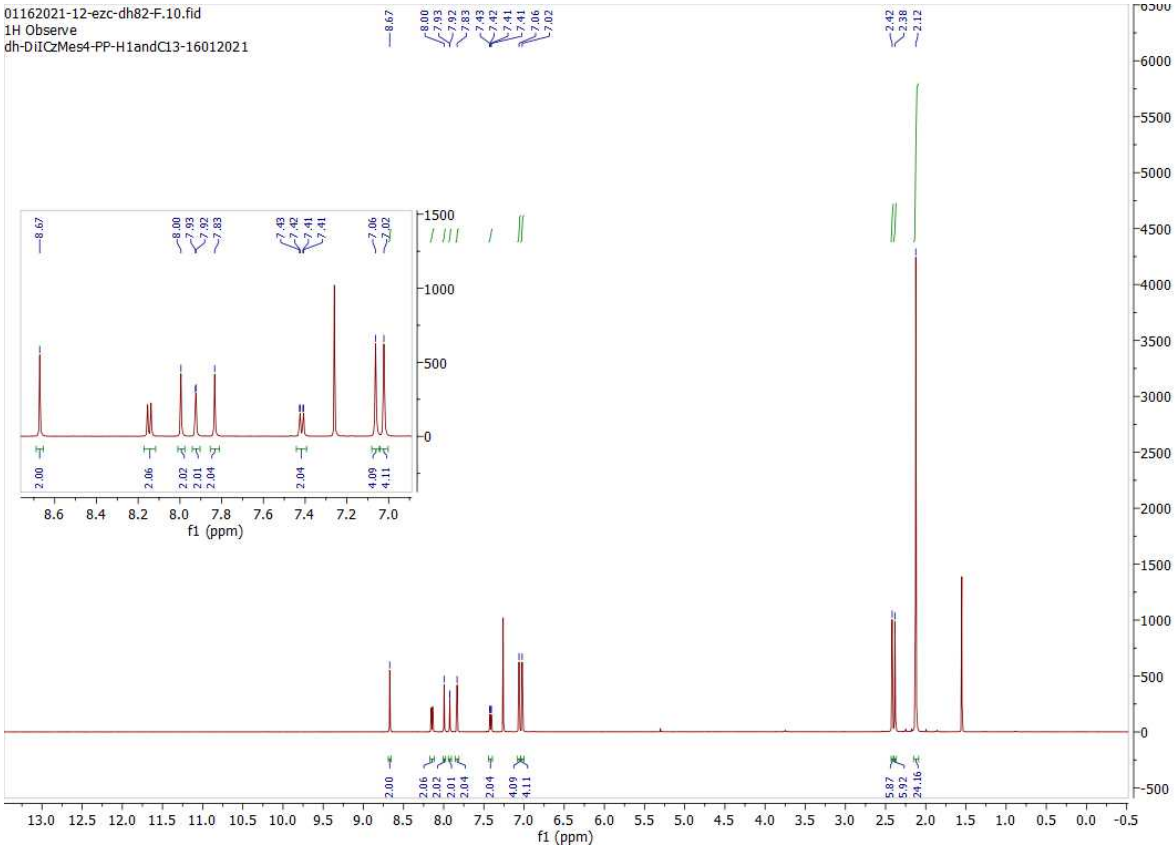

Figure **S20**. ^{1}H NMR of **DiICzMes$_4$** in $CDCl_3$.

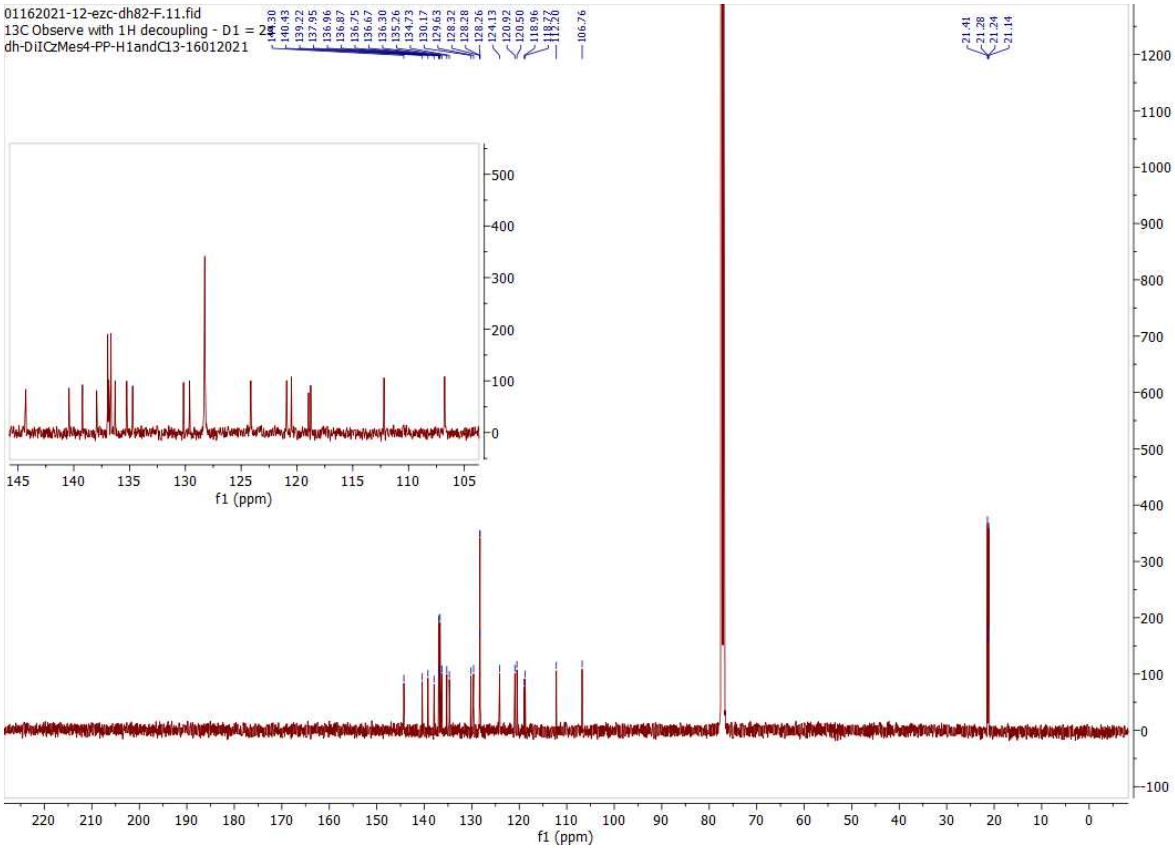

Figure **S21**. ^{13}C NMR of **DiICzMes$_4$** in $CDCl_3$.

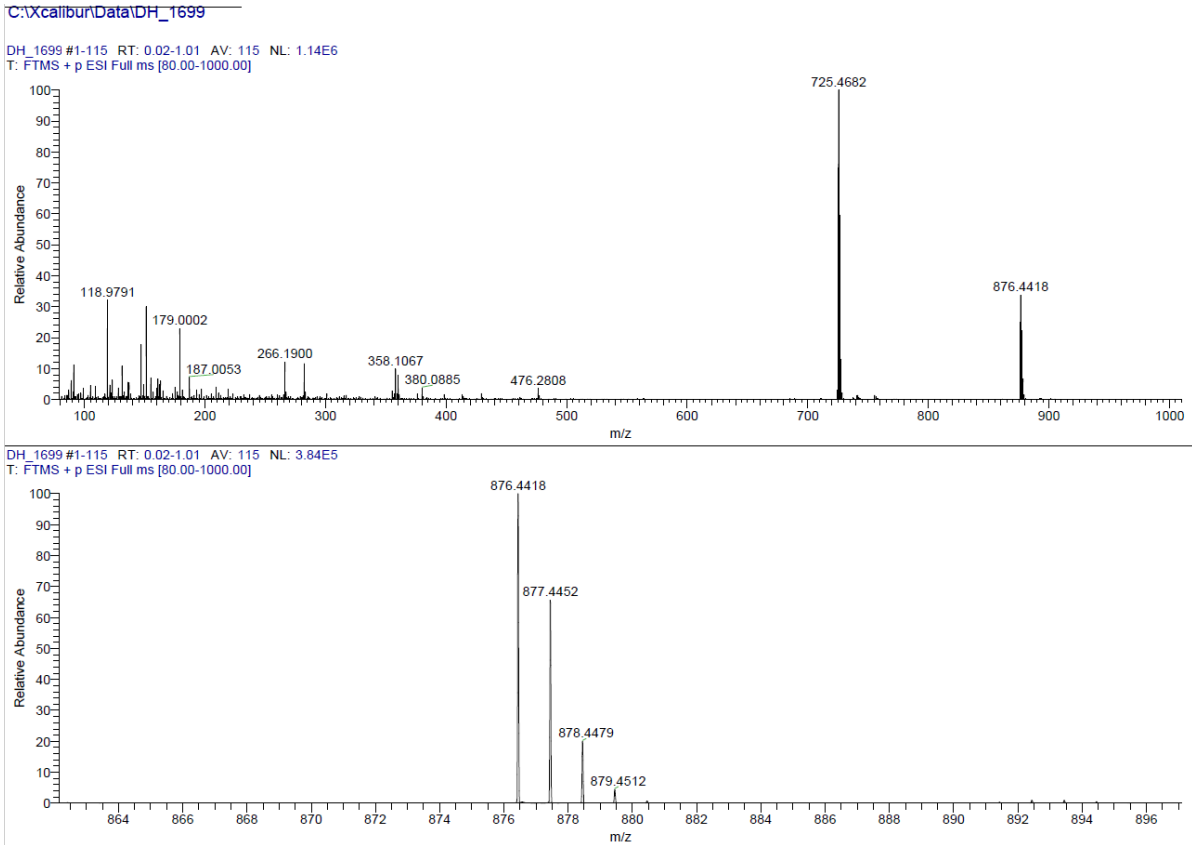

Figure **S22**. HRMS of **DiICzMes$_4$.**

HPLC Trace Report04Apr2021

<Sample Information>

Sample Name	: diicz-col-1s rc		
Sample ID	:		
Method Filename	: 85% Methanol 15% THF 20 mins.lcm		
Batch Filename	: 02042021.lcb		
Vial #	: 1-21	Sample Type	: Unknown
Injection Volume	: 8 uL		
Date Acquired	: 02/04/2021 18:23:21	Acquired by	: System Administrator
Date Processed	: 02/04/2021 18:43:22	Processed by	: System Administrator

<Chromatogram>

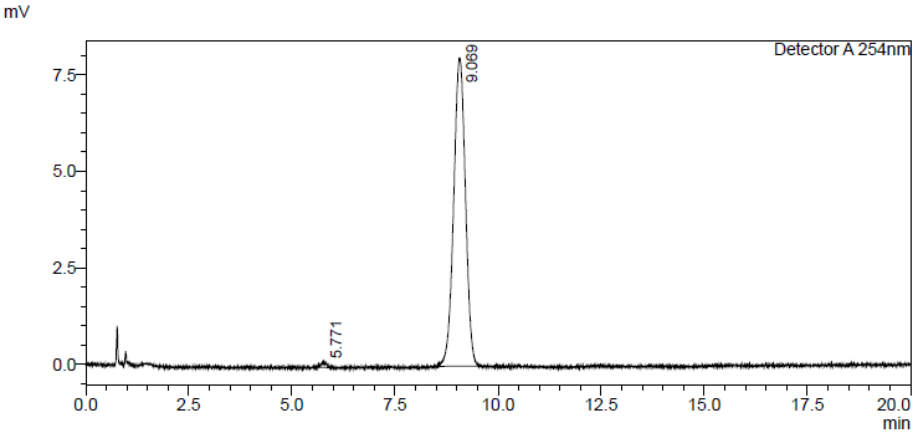

<Peak Table>

Detector A 254nm

Peak#	Ret. Time	Area	Height	Area%	Area/Height	Width at 5% Height
1	5.771	1335	120	0.835	11.087	0.312
2	9.069	158509	7981	99.165	19.860	0.660
Total		159844	8102	100.000		

Figure **S23**. HPLC trace report for **DiICzMes$_4$**.

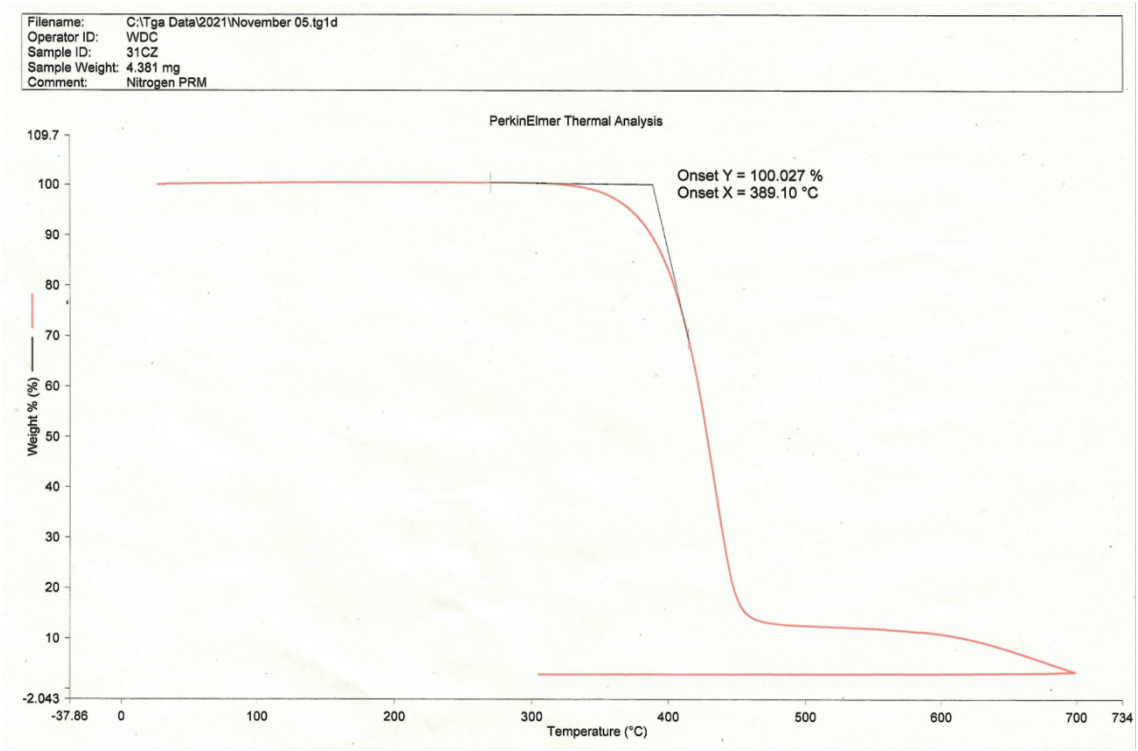

a

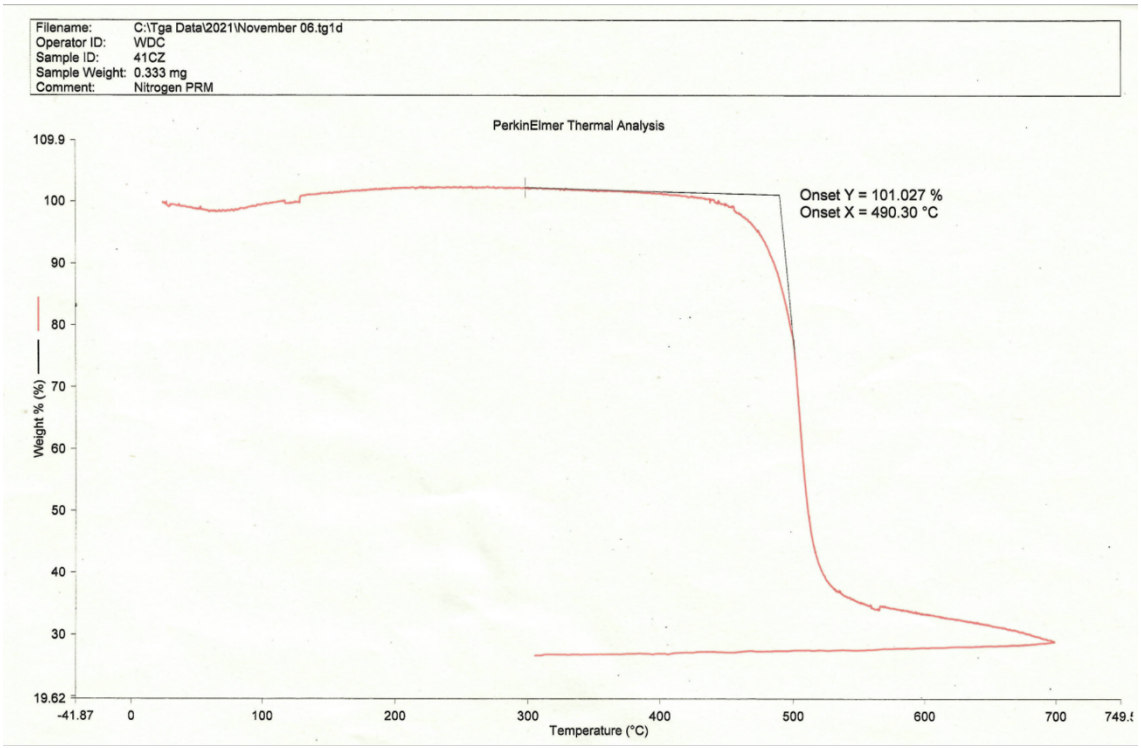

b

Figure **S24.** TGA of(**a**) **ICzMes$_3$** and (**b**) **DiICzMes$_4$**.

X-ray Crystallography

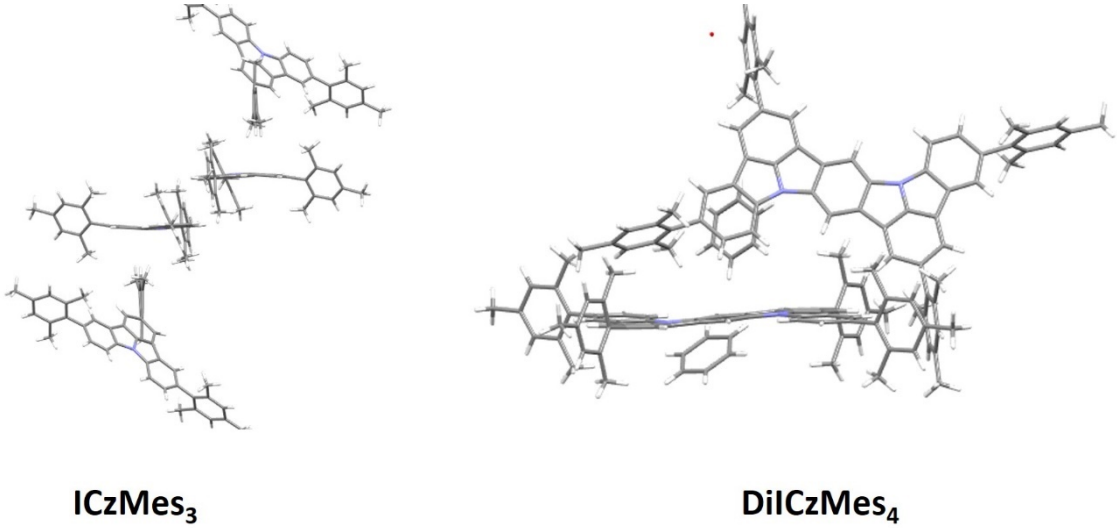

Figure **S25**. Packing regimes of **ICzMes$_3$** and **DiICzMes$_4$**.

Single-crystal X-ray diffraction data were collected with a Rigaku MM007 HF and Pilatus detector d with Cu-Kα radiation. The structures were solved by direct methods and refined on F^2 by using SHELXL. These data can be obtained free of charge via www.ccdc.cam.ac.uk/conts/retrieving.html or from the Cambridge Crystallographic Data centre, 12 Union Road, Cambridge CB2 1EZ, UK; fax (+44) 1223-336-033; e-mail: deposit@ccdc.cam.ac.uk. CCDC Nos 2104486 and 2104487

Table **S4**. Selected crystallographic data.

	ICzMes$_3$	**DiICzMes$_4$**
Empirical formula	$C_{45}H_{41}N$	$C_{75}H_{67}N_2O$
Formula Weight	595.83	1012.37
Crystal color, Habit	Colourless, prism	Yellow, prism
Crystal Dimensions / mm^3	0.13 × 0.02 × 0.02	0.20 × 0.05 × 0.05
Crystal System	Monoclinic	Triclinic
Lattice type	Primitive	Primitive
a / Å	8.24799(12)	13.33760(16)
b / Å	14.19010(18)	15.89840(19)
c / Å	28.3417(4)	16.118(2)
α / °		86.2207(10)
β / °	90.5962(13)	87.3777(10)
Γ / °		69.0861(11)
V / Å^3	3316.93(8)	3302.08(7)
Space Group	$P2_1/n$(#14)	P-1 (#2)
Z value	4	2
D_{calc} / g cm^{-3}	1.193	1.018
F_{000}	1272.00	1078.00
μ(CuKα) / cm^{-1}	5.122	4.507

Diffractometer	XtaLAB P100	XtaLAB P200
Radiation	CuKα (λ = 1.54184 Å) multi-layered mirror monochromated	CuKα (λ = 1.54184 Å) multi-layered mirror monochromated
Temperature / °C	-100.00	-148.0
Detector Aperture / mm	83.8 × 33.5	83.8 × 70.0
Data Images	3982 exposures	
Pixel Size / mm	0.172	
$2\theta_{max}$ / °	136.6	151.0
No. of reflections measured	Total: 34062 Unique: 5985 (R_{int} = 0.0389)	Total: 37140 Unique: 12877 (R_{int} = 0.0122)
Corrections	Lorentz-polarization Absorption (trans. Factors:0.641-0.990)	Lorentz-polarization Absorption (trans. Factors:0.766-0.978) Secondary Extinction (coefficient: 2.79100e-002
Structure Solution	Direct Methods (SHELXT version 2018/2)	Direct Methods (SHELXT version 2018/2)
Refinement	Full-matrix least-squares on F^2	Full-matrix least-squares on F^2
Function Minimized	$\Sigma\ w\ (Fo^2 - Fc^2)^2$	$\Sigma\ w\ (Fo^2 - Fc^2)^2$
Least squares weights	$w = 1/[\sigma^2(Fo^2) + (0.0682 \cdot P)^2 + 1.1538 \cdot P]$ Where $P = (Max(Fo^2,0) + 2Fc^2)/3$	$w = 1/[\sigma^2(Fo^2) + (0.2000 \cdot P)^2 + 0.0000 \cdot P]$ Where $P = (Max(Fo^2,0) + 2Fc^2)/3$
$2\theta_{cutoff}$ / °	136.6	151.0
Anomalous Dispersion	All non-hydrogen atoms	All non-hydrogen atoms
No. Observations (All reflections)	5985	12877
No. Variables	424	728
Reflection/Parameter ratio	14.12	17.69
Residuals: R1(I>2.00σ(I))	0.0424	0.1510
Residuals: R (All reflections)	0.0463	0.1545
Residuals: wR2 (All reflections)	0.1187	0.5275
Goodness of Fit indicator	0.996	2.941
Max Shift/Error in Final cycle	0.000	0.170
Maximum peak in Final Diff. Map	$0.24e^-/Å^3$	$1.66e^-/Å^3$
Minimum peak in Final Diff. Map	$-0.24e^-/Å^3$	$-0.84e^-/Å^3$

Computations

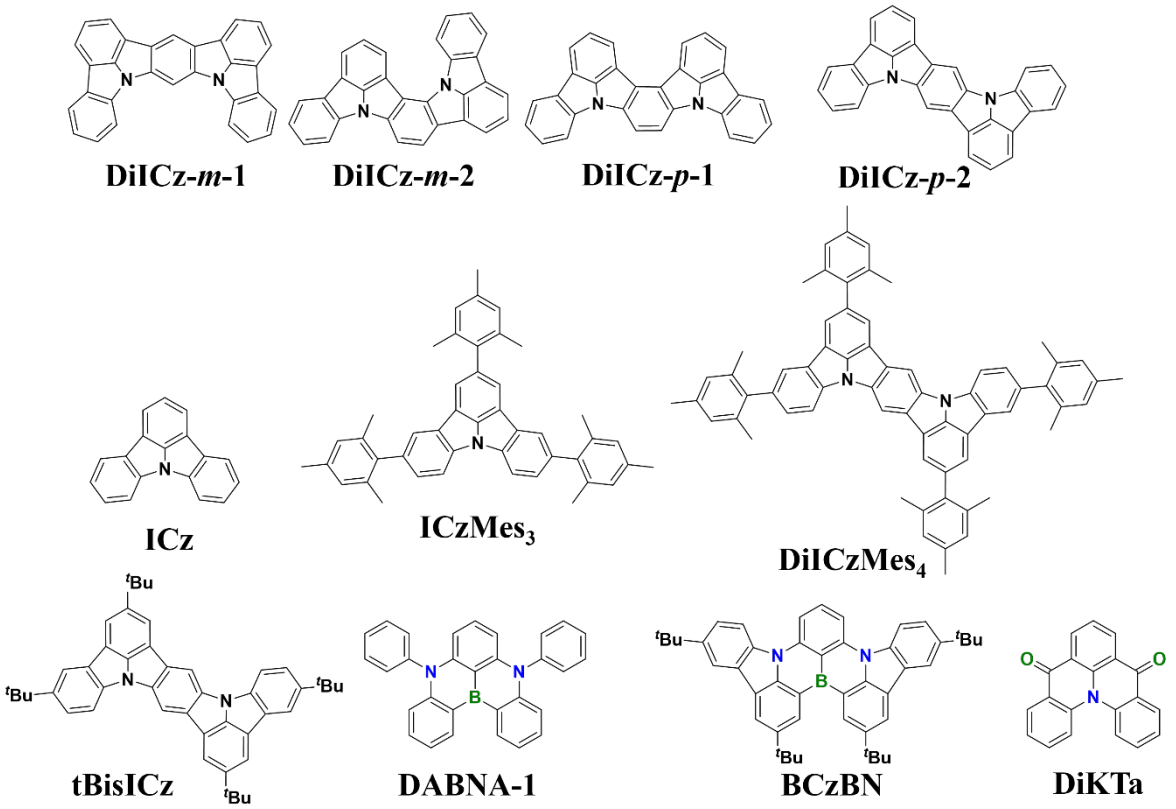

Figure **S26.** Structures of modelled compounds.

Table **S5**. HOMO and LUMO energies of the investigated compounds at PBE0/6-31G(d,p) level, in the gas phase.

Compound	HOMO / eV	LUMO / eV	Δ*E* / eV
ICz	-5.84	-1.19	4.65
DiICz-*m*-1	-5.63	-1.31	4.32
DiICz-*m*-2	-5.68	-1.35	4.33
DiICz-*p*-1	-5.53	-1.51	4.02
DiICz-*p*-2	-5.50	-1.55	3.95
ICzMes$_3$	-5.78	-1.28	4.50
DiICzMes$_4$	-5.48	-1.62	3.86
tBisICz	-5.29	-1.44	3.85
DABNA-1	-4.99	-1.01	3.98
BCzBN	-5.30	-1.70	3.60
DiKTa	-6.20	-2.23	3.97

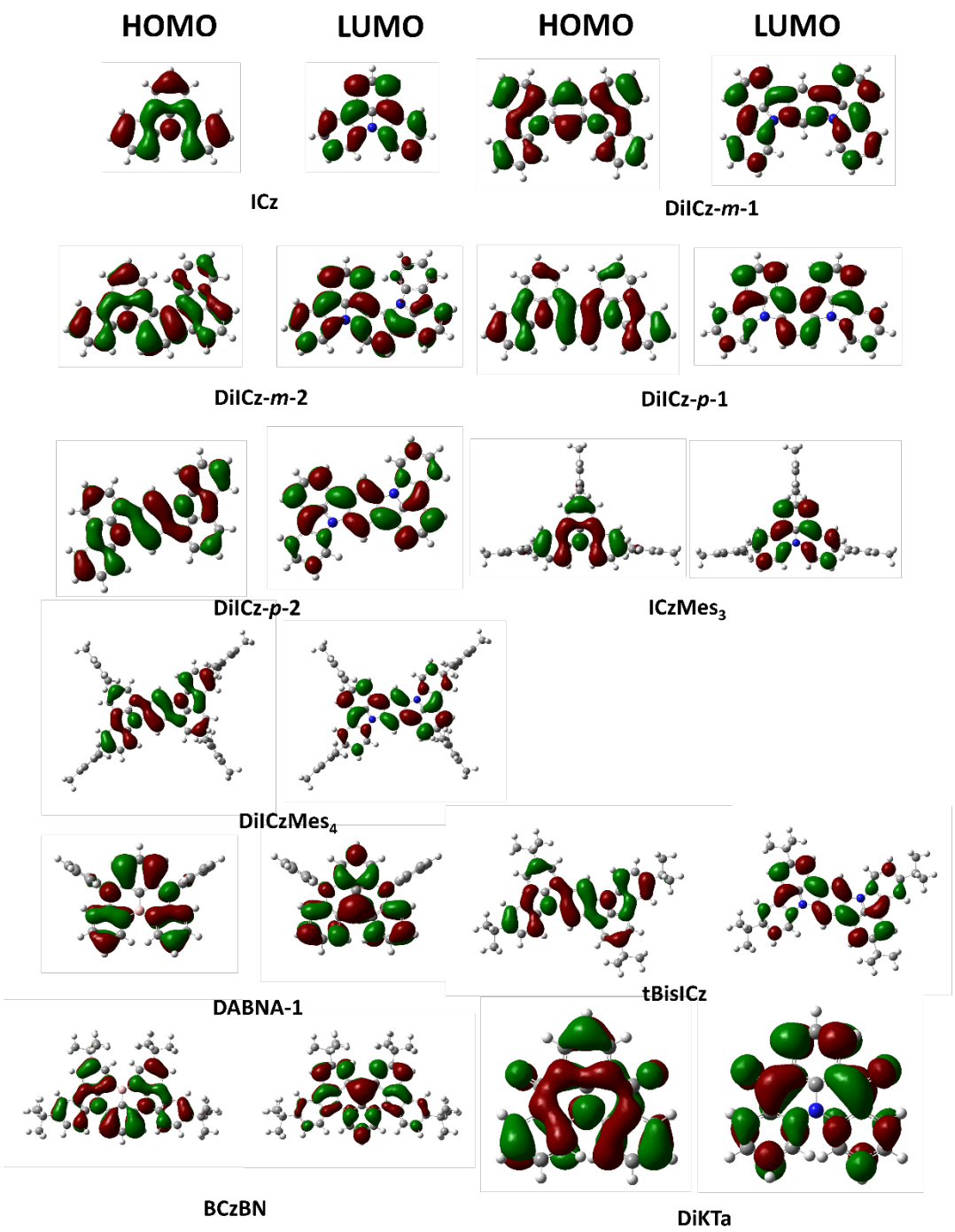

Figure **S27**. HOMO and LUMO electron density distributions of each modelled material, calculated at the PBE0/6-31G(d,p) level, isovalue = 0.02.

Table **S6**. Calculated vertical excited energies of proposed structures from the ground state geometry at SCS-CC2/cc-pVDZ

Compound	**S_1 (*f*) / eV**	**S_2 (*f*) / eV**	**T_1 / eV**	**T_2 / eV**	**ΔE_{ST} / eV**
ICz	3.78 (0.10)	4.34 (0.09)	3.45	3.63	0.33
DiICz-*m*-1	3.58 (0.18)	3.91 (0.04)	3.29	3.42	0.30
DiICz-*m*-2	3.57 (0.12)	3.86 (0.34)	3.26	3.42	0.32
DiICz-*p*-1	3.36 (0.01)	3.75 (0.65)	3.19	3.22	0.17
DiICz-*p*-2	3.31 (0.15)	3.95 (0.52)	3.17	3.18	0.15

f is oscillator strength

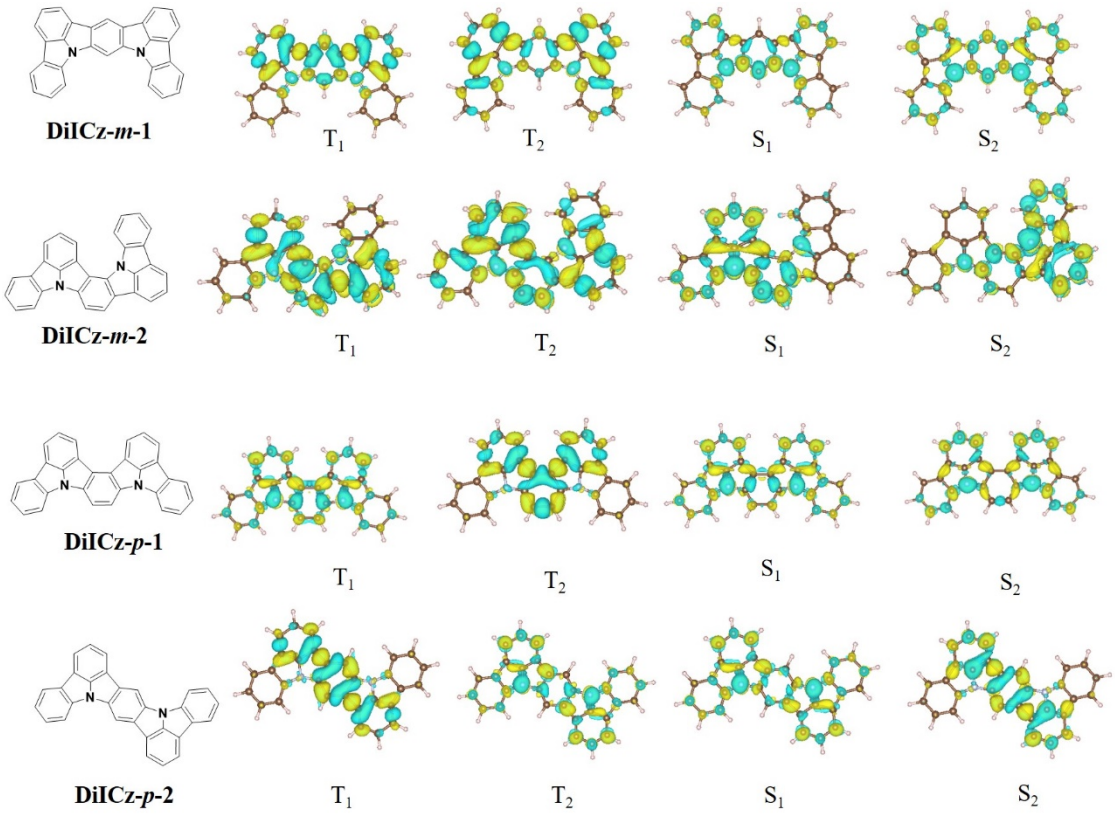

Figure **S28**. Difference density plots of the proposed targets computed at the SCS-CC2/cc-pVDZ level of theory from vertical excitation from the ground state.

Table **S7**. Calculated vertical excited energies of emitters and MR-TADF emitters previously reported in the literature at SCS-CC2/cc-pVDZ level of theory from vertical excitation from the ground state.

Compound	**S_1 (*f*) / eV**	**S_2 (*f*) / eV**	**T_1 / eV**	**T_2 / eV**	**ΔE_{ST} / eV**
ICz	3.78 (0.10)	4.34 (0.09)	3.45	3.63	0.33
ICzMes$_3$	3.64 (0.14)	4.19 (0.13)	3.42	3.50	0.21
DiICzMes$_4$	3.21 (0.21)	3.83 (0.66)	3.08	3.14	0.13
tBisICz	3.21 (0.18)	3.87 (0.55)	3.07	3.16	0.14
DABNA-1	3.26 (0.31)	4.20 (0.04)	3.10	3.85	0.16
BCzBN	2.96 (0.54)	3.63 (0.02)	2.87	3.26	0.09
DiKTa	3.45 (0.20)	3.92 (0.00)	3.18	3.60	0.27

f is oscillator strength

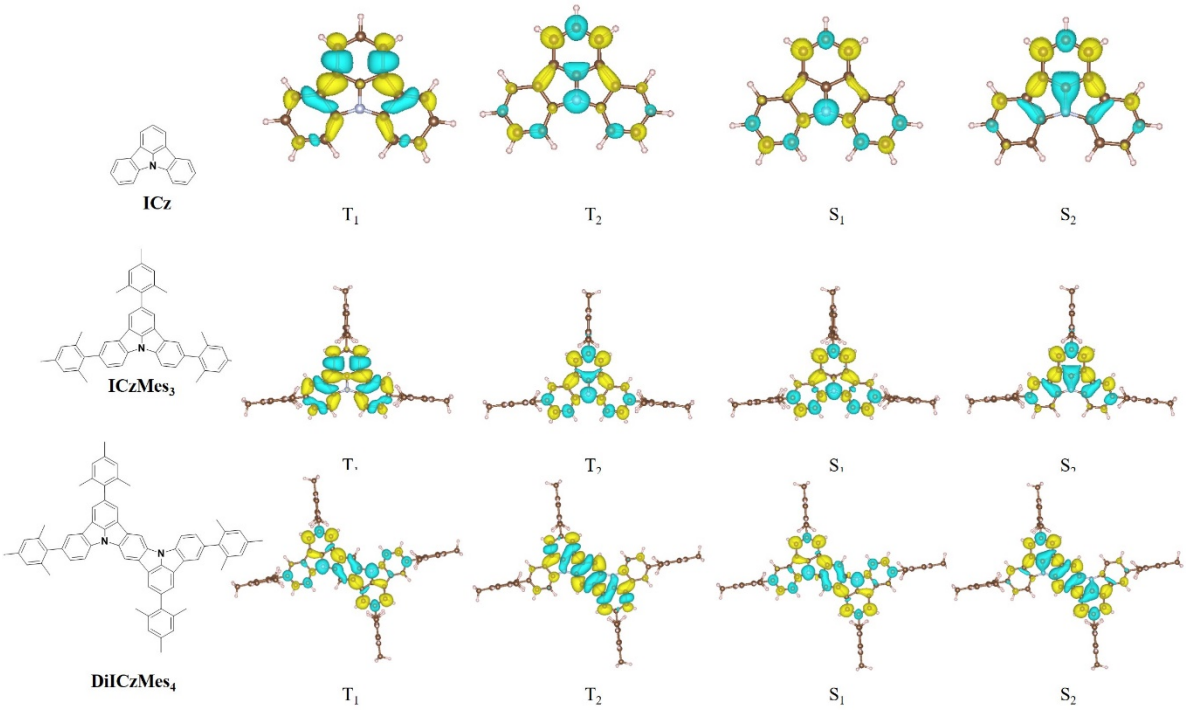

Figure **S29**. Difference density plots of our emitters calculated at the SCS-CC2/cc-pVDZ level of theory from vertical excitation from the ground state.

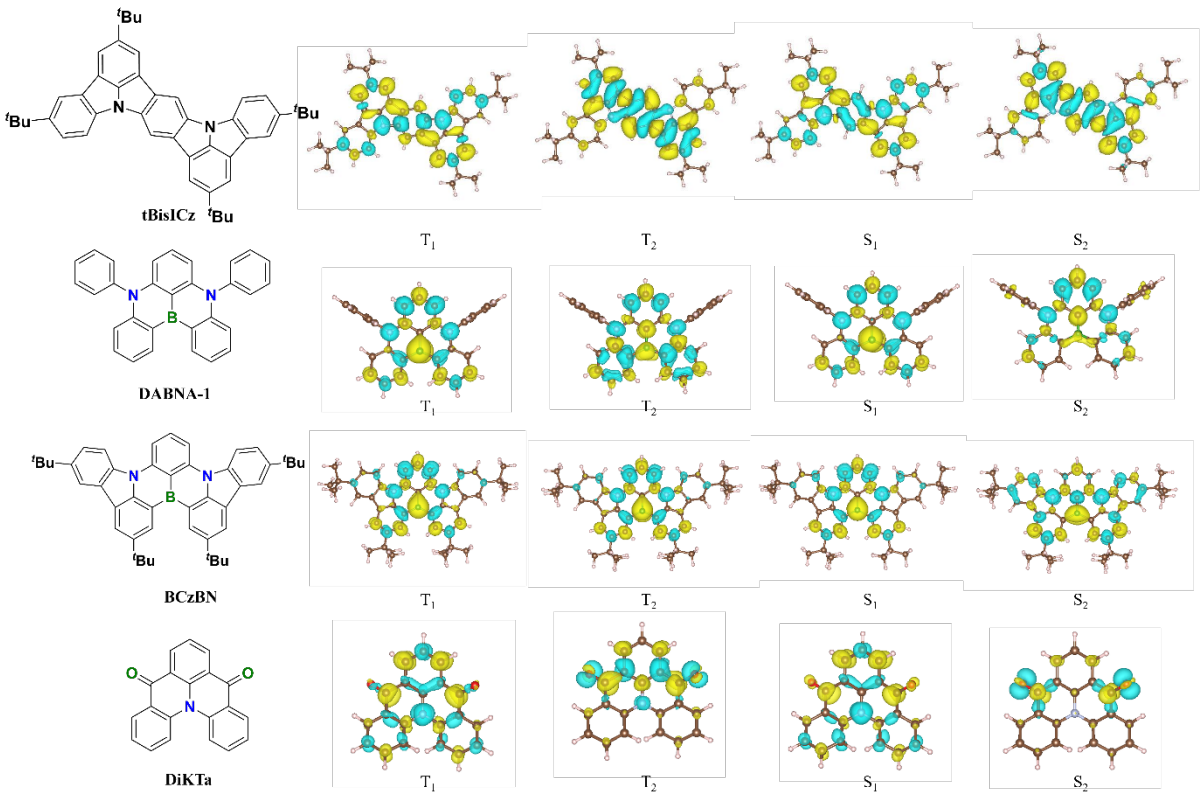

Figure **S30**. Difference density plots of literature emitters calculated at the SCS-CC2/cc-pVDZ level of theory from vertical excitation from the ground state.

Table **S8**. SCS-CC2/cc-pVDZ calculated S_1 and T_1 energies of the target emitters and previously reported MR-TADF emitters from TDA/PBE0 6-31G(d,p) optimized excited states.

Compound	**S_1 (f) / eV[a]**	**T_1 / eV[b]**	**ΔE_{ST} / eV**
ICz	3.59 (0.04)	2.99	0.59
ICzMes$_3$	3.42 (0.07)	2.97	0.45
DiICzMes$_4$	3.06 (0.11)	2.78	0.29
tBisICz	3.07 (0.09)	2.77	0.30
DABNA-1	3.14 (0.24)	3.02	0.12
BCzBN	2.90 (0.49)	2.81	0.09
DiKTa	3.31 (0.17)	3.04	0.26

[a]From S_1 TDA/PBE0, 6-31G(d,p) optimized geometry, [b]From T_1 TDA/PBE0 6-31G(,d,p) optimized geometry, f is oscillator strength.

Table **S9**. Changes in S_1 and T_1 energies between Ground state and optimized excited geometries

Compound	**S_1 (*f*) / eV[a]**	**S_1 (*f*)/ eV[b]**	**λ_{S1} / eV[c]**	**T_1 / eV[d]**	**T_1 / eV[e]**	**λ_{T1} / eV[f]**
ICz	3.78 (0.10)	3.59 (0.04)	0.19	3.45	2.99	0.46
ICzMes$_3$	3.64 (0.14)	3.42 (0.07)	0.22	3.42	2.97	0.45
DiICzMes$_4$	3.21 (0.21)	3.06 (0.11)	0.15	3.08	2.78	0.30
tBisICz	3.21 (0.18)	3.07 (0.09)	0.14	3.07	2.77	0.30
DABNA-1	3.26 (0.31)	3.14 (0.24)	0.12	3.10	3.02	0.08
BCzBN	2.96 (0.54)	2.90 (0.49)	0.06	2.87	2.81	0.06
DiKTa	3.45 (0.20)	3.31 (0.17)	0.14	3.18	3.04	0.14

[a]From S_1 SCS-CC2/cc-pVDZ optimized geometry, [b]From TDA/PBE0, 6-31G(d,p) optimized geometry, [c]From a - b, [d]From S_1 SCS-CC2/cc-pVDZ optimized geometry, [e]From TDA/PBE0, 6-31G(d,p) optimized geometry, [f]From d - e, , *f* is oscillator strength.

Table **S10**. Density data calculated from vertical excitation at SCS-CC2/cc-pVDZ.

	Ground state geometry[a]			**Optimized excited state geometry[b]**		
Compound	**CT[c]**	**D_CT[d]**	**Overlap[e]**	**CT[c]**	**D_CT[d]**	**Overlap[e]**
ICz S_1	0.489	1.251	0.935	0.596	2.073	0.719
ICz T_1	0.279	0.350	0.984	0.284	0.407	0.976
ICzMes$_3$ S_1	0.503	1.266	0.937	0.600	2.126	0.705
ICzMes$_3$ T_1	0.283	0.295	0.987	0.341	0.745	0.962
DiICzMes$_4$ S_1	0.522	0.001	0.956	0.557	0.002	0.921
DiICzMes$_4$ T_1	0.539	0.000	0.970	0.463	0.000	0.862

[a]Caclulated from ground state optimized geometry, SCS-CC2/cc-pVDZ, [b]Calculated from the excited state optimized geometry, PBE0/6-31G(d,p), [c]Charge transfer between area of increased and decreased density, [d]Distance of charge transferred between area of increased and decreased density, [e]Overlap between areas of increased and decreased density.

Table **S11**. Calculated and experimental ΔE_{ST} values of the emitters and literature cores.

Compound	**ΔE_{ST}-Vert / eV[a]**	**ΔE_{ST}-Ad / eV[b]**	**$\Delta\Delta E_{ST}$ / eV[c]**	**ΔE_{ST}-Exp / eV[d]**
ICz	0.33	0.59	0.26	0.47
$ICzMes_3$	0.21	0.45	0.24	0.39
$DiICzMes_4$	0.13	0.29	0.16	0.26
tBisICz	0.14	0.30	0.16	0.29[e]
DABNA-1	0.16	0.12	-0.04	0.15[f]
BCzBN	0.09	0.09	0.00	0.12
DiKTa	0.27	0.26	-0.01	0.18

[a]Computed at the SCS-CC2/cc-pVDZ level of theory from vertical excitation of the ground state geometry SCS-CC2, [b]Computed from vertical exaction of the S_1 and T_1 optimized excited state geometries, [c]Difference between ΔE_{ST} computed in a and b, [d]From onset of fluoresence and phosphorescence in dilute toluene at 77 K, [e]Obtained in 1 wt% mCP:TSPO1 film, [f]Obtained in EtOH.

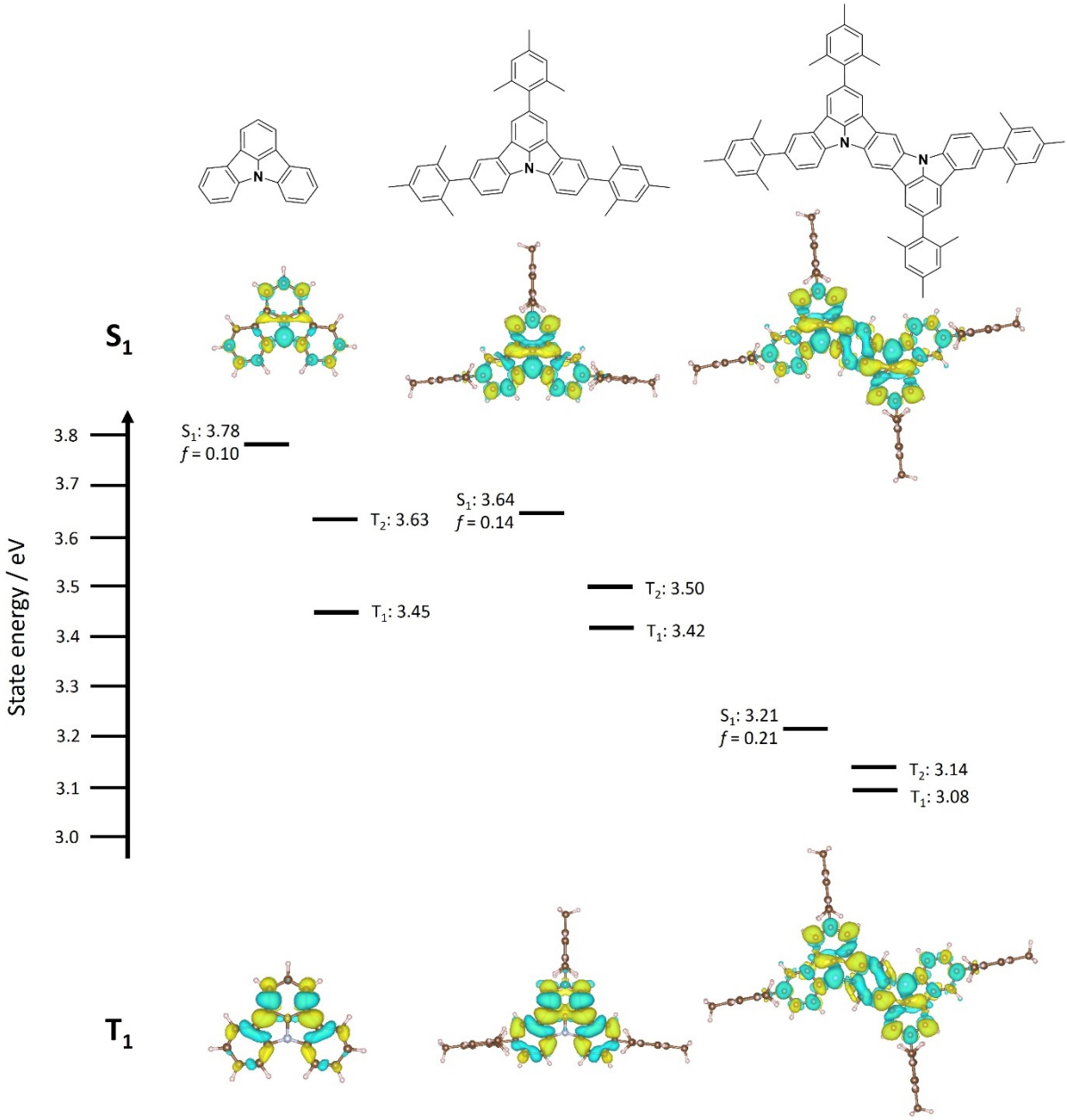

Figure **S31**. Structures, excited state energies and difference density plots of each S_1 and T_1 for **ICz** (left panel), **ICzMes$_3$** (central panel) and **DiICzMes$_4$** (right panel) from the ground state optimized geometries.

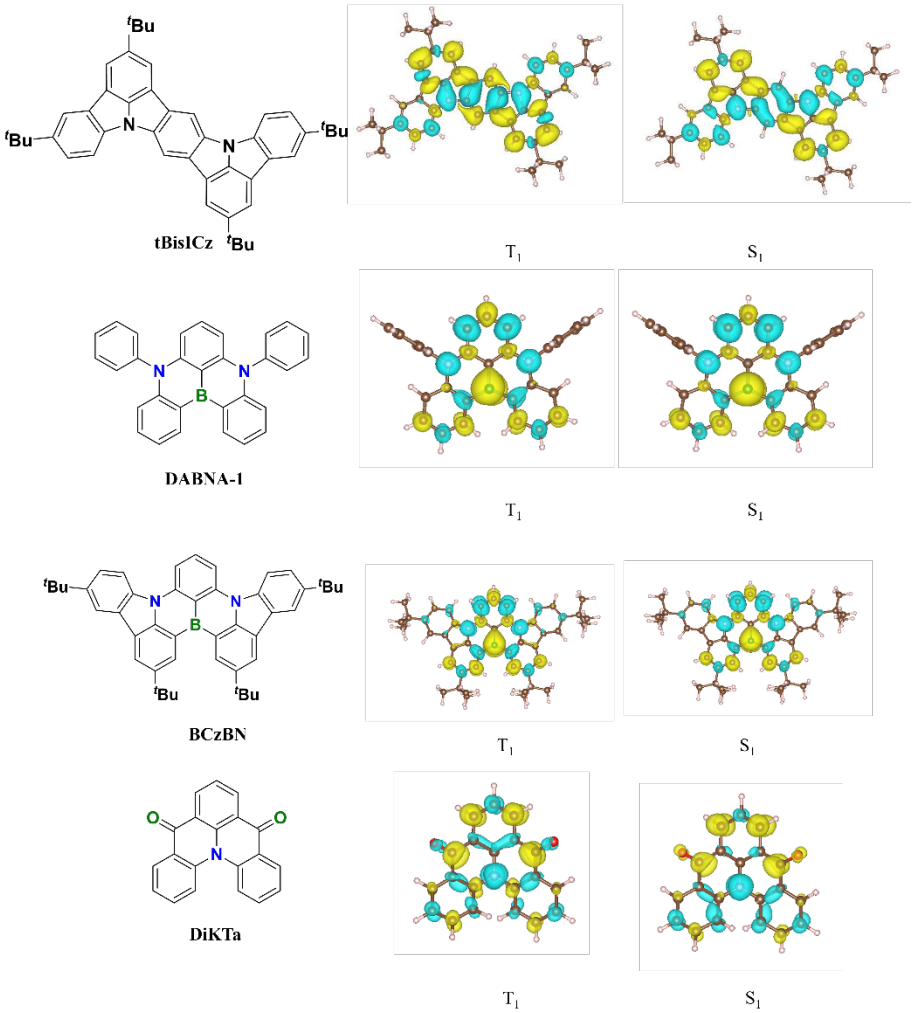

Figure **S32**. Difference density plots of literature emitters for S_1 and T_1 excited states computed at the SCS-CC2/cc-pVDZ level of theory based on excited states optimization carried out at the TDA/PBE0/6-31G(d,p) level of theory.

Optoelectronic data

In detail, the contribution of PF and DF to the total experimentally measured quantum yield were determined by[37]

$$\text{PF} = \frac{A_{PF} \times \tau_{PF}}{(A_{PF} \times \tau_{PF}) + (A_{DF} \times \tau_{DF})} \quad (1) \qquad \text{DF} = \frac{A_{DF} \times \tau_{DF}}{(A_{DF} \times \tau_{DF}) + (A_{PF} \times \tau_{PF})} \quad (2)$$

Rate constants were calculated according to methods described by.[38]

Where k_p and k_d are the prompt and delayed fluorescent rates, and k_{ISC} and k_{RISC} are the intersystem and reverse intersystem crossing rates calculated by:

$$k_p = 1 \div \tau_p \ (4) \qquad k_d = 1 \div \tau_d \ (5)$$

$$k_{ISC} = k_p \times (1 - \Phi_p) \ (6)$$

$$k_{RISC} = \frac{k_p \times k_d}{k_{ISC}} \left(\frac{\Phi_d}{\Phi_p}\right) \ (7)$$

Table **S12**. Electrochemical data of each emitter

Compound	**E^{ox} [a] / V**	**E^{red} [b] / V**	**HOMO [c] / eV**	**LUMO [c] / eV**	**ΔE_{H-L} [d] / eV**
ICz	1.45	-2.21	-5.79	-2.14	3.61
ICzMes$_3$	1.43	-2.16	-5.77	-2.19	3.58
DiICzMes$_4$	1.11	-1.92	-5.45	-2.43	3.02

[a]Reported versus SCE in degassed DCM with 0.1 M [nBu$_4$N]PF$_6$ as the supporting electrolyte and Fc/Fc$^+$ as the internal reference (0.46 V vs. SCE) calculated from DPV.[1] [b]Reported versus SCE in degassed DMF with 0.1 M [nBu$_4$N]PF$_6$ as the supporting electrolyte and Fc/Fc$^+$ as the internal reference (0.45 V vs. SCE) calculated from DPV,[1] [c]The HOMO and LUMO energies were determined using the relation $E_{HOMO/LUMO} = -(E^{ox} / E^{red} + 4.8)$ eV,[2] where E^{ox} and E^{red} are the anodic and cathodic peak potentials, respectively calculated from DPV related to Fc/Fc$^+$. [d] $E_{H-L} = |E_{HOMO} - E_{LUMO}|$.

Table **S13**. Solvatochromic study of **ICz**

Solvent	λ^a (ε) / nm (/ 10^4 M^{-1} cm^{-1})	$\lambda_{PL}{}^b$ / nm	FWHM / nm (eV)	Stokes shift / nm
PhMe	364 (9), 350 (6), 320 (7), 309 (6), 292 (10), 285 (31)	374	21 (0.18)	10
2-MeTHF	362 (12), 347 (8), 319 (10), 307 (9), 291 (12), 284 (42)	372	22 (0.19)	10
EtOAc	362 (9), 348 (6), 319 (7), 307 (7), 292 (8), 284 (33)	372	24 (0.21)	10
DCM	363 (8), 348 (5), 320 (7), 308 (6), 292 (8), 285 (28)	376	26 (0.22)	13
DMF	362 (9), 347 (6), 319 (7), 306 (6), 291 (9), 285 (29)	377	28 (0.24)	15

[a] Obtained under aerated conditions at 298 K. [b] Concentration 0.6 - 2 x 10^{-5} M, λ_{exc} = 320 nm

Table **S14**. Solvatochromic study of **ICzMes$_3$**

Solvent	λ^a (ε) / nm (/ 10^4 M^{-1} cm^{-1})	$\lambda_{PL}{}^b$ / nm	FWHM / nm (eV)	Stokes shift / nm
PhMe	379 (8), 363 (6), 330 (8), 318 (6), 300 (14), 291 (40)	387	21 (0.17)	8
2-MeTHF	377 (13), 361 (10), 329 (13), 316 (10), 299 (20), 290 (65)	387	22 (0.18)	10
EtOAc	376 (10), 360 (7), 328 (9), 315 (7), 298 (14), 289 (50)	387	25 (0.20)	11
DCM	377 (15), 362 (11), 329 (14), 316 (12), 290 (72)	389	28 (0.22)	12
DMF	376 (12), 358 (8), 329 (11), 315 (9), 298 (21), 290 (60)	391	30 (0.23)	15

[a] Obtained under aerated conditions at 298 K. [b] Concentration 0.6 - 2 x 10^{-5} M, λ_{exc} = 320 nm

Table **S15**. Solvatochromic study of **DiICzMes$_4$**

Solvent	λ^a (ε) / nm (/ × 10^4 M^{-1} cm^{-1})	$\lambda_{PL}{}^b$ / nm	FWHM / nm (eV)	Stokes shift / nm
PhMe	431 (11), 410 (8), 365 (39), 345 (19), 316 (59), 307 (62), 302 (58)	441	17 (0.11)	10
2-MeTHF	429 (14), 409 (11), 363 (46), 344 (24), 314 (66), 305 (74), 299 (70)	439	18 (0.12)	10
EtOAc	428 (18), 407 (14), 362 (59), 342 (32), 313 (89), 304 (103), 299 (99)	439	18 (0.12)	11
DCM	430 (16), 409 (13), 364 (53), 344 (29), 315 (81), 306 (88), 300 (84)	441	20 (0.13)	11
DMF	429 (13), 409 (10), 363 (40), 344 (22), 314 (63), 305 (69), 300 (65)	442	20 (0.13)	13

[a] Obtained under aerated conditions at 298 K. [b] Concentration 0.6 - 2 x 10^{-5} M, λ_{exc} = 380 nm

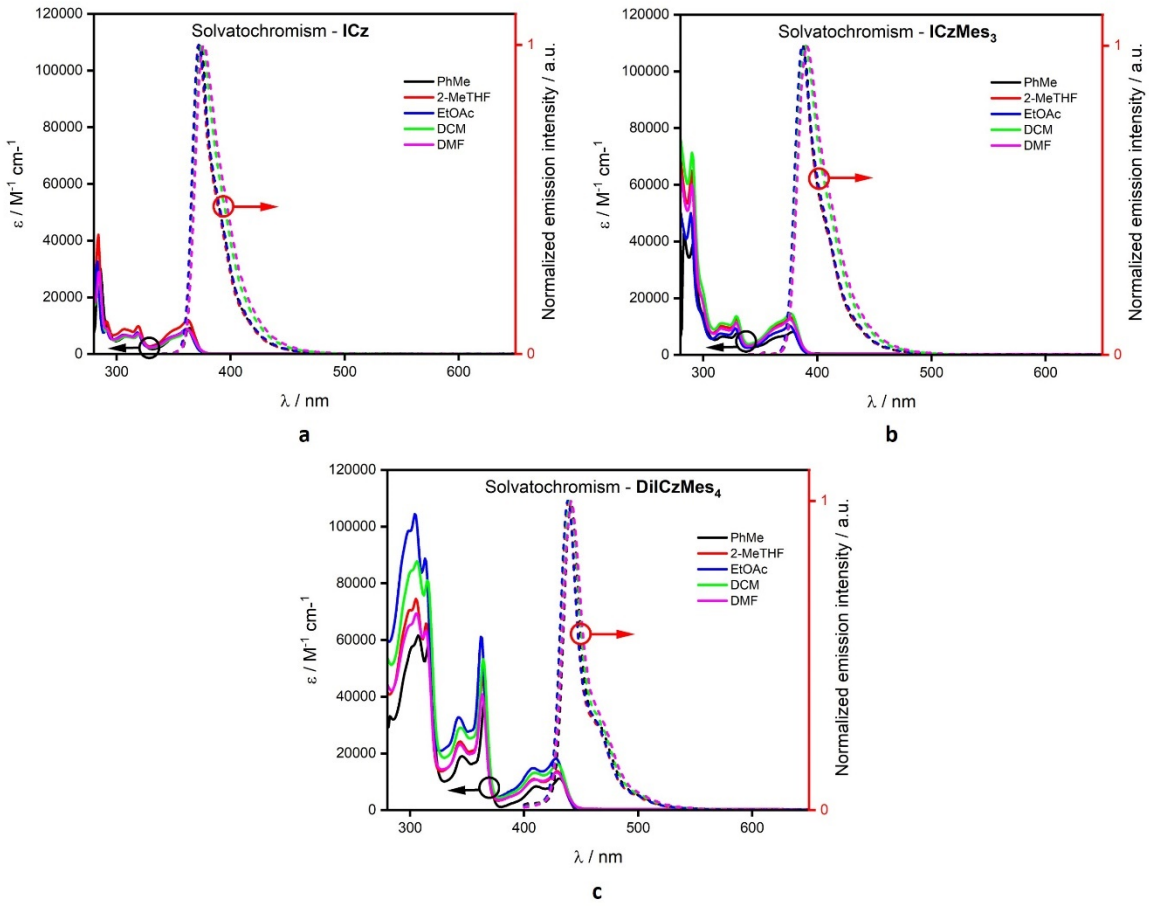

Figure **S33**. Solvatochromism screen of (**a**) **ICz**, (**b**) **ICzMes$_3$** and (**c**) **DiICzMes$_4$**, where PhMe, 2-MeTHF, EtOAc, DCM and DMF are toluene, 2-methyltetrahydrafuran, ethyl acetate, 1,2-dichloromethane and dimethylformamide respectively, **ICz** and **ICzMes$_3$** λ_{exc} = 320 nm, **DiICzMes$_4$** λ_{exc} = 380 nm.

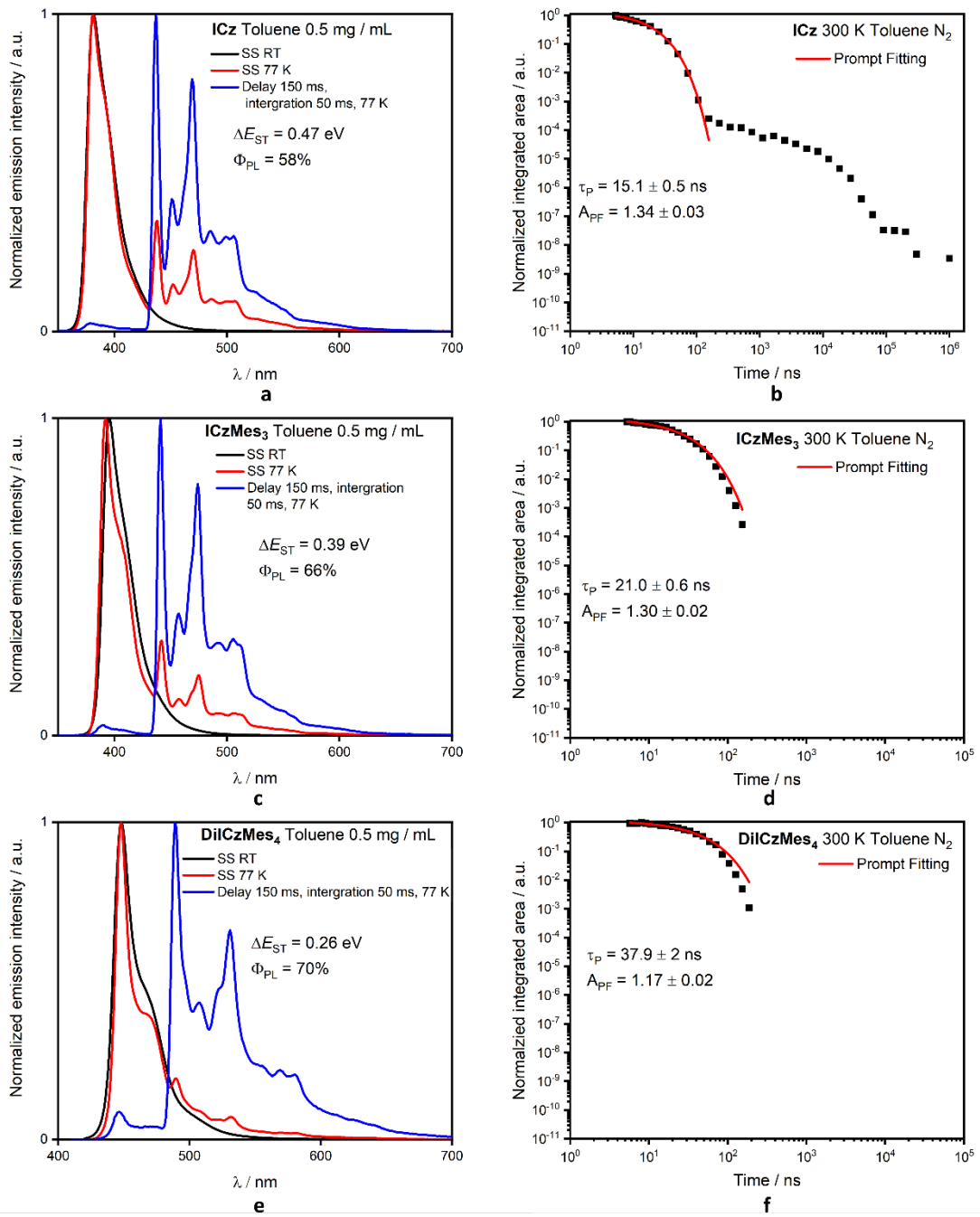

Figure **S34**. Solution-state photophysical data in toluene, emission spectra (**a**, **c**, **e**) steady-state at RT, 77 K and gated emission, λ_{exc} = 330 nm, and transient PL (**b**, **d**, **f**) at 300 K, λ_{exc} = 355 nm, with mono exponential fitting of the decays of **ICz** (**a** and **b**), **ICzMes$_3$** (**c** and **d**), **DiICzMes$_4$** (**e** and **f**).

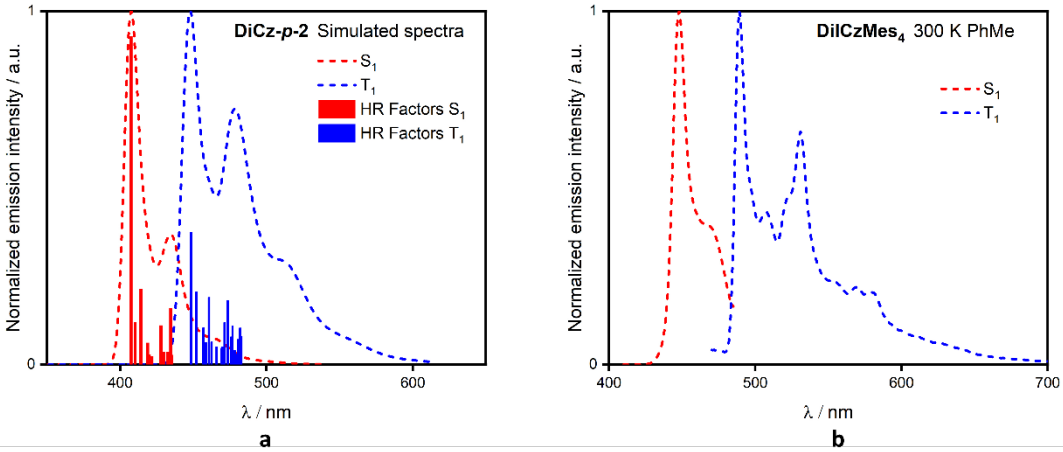

Figure **S35**.Singlet and triplet spectra from **a**) simulated emission spectra of **DiCz-*p*-2**, Undistorted displaced harmonic oscillator model. The vertical bars show the Huang-Rhys factors for the most strongly coupled vibrational modes, calculated at TDA/DFT/PBE0/6-31G(d,p), **b**) spectra of **DiICzMes4** in toluene at 77 K, where S_1 is assigned from the SS spectrum at 77 K and T_1 from the delayed emission spectrum (150 ms delay and 50 ms integration), where overlapping components have been omitted.

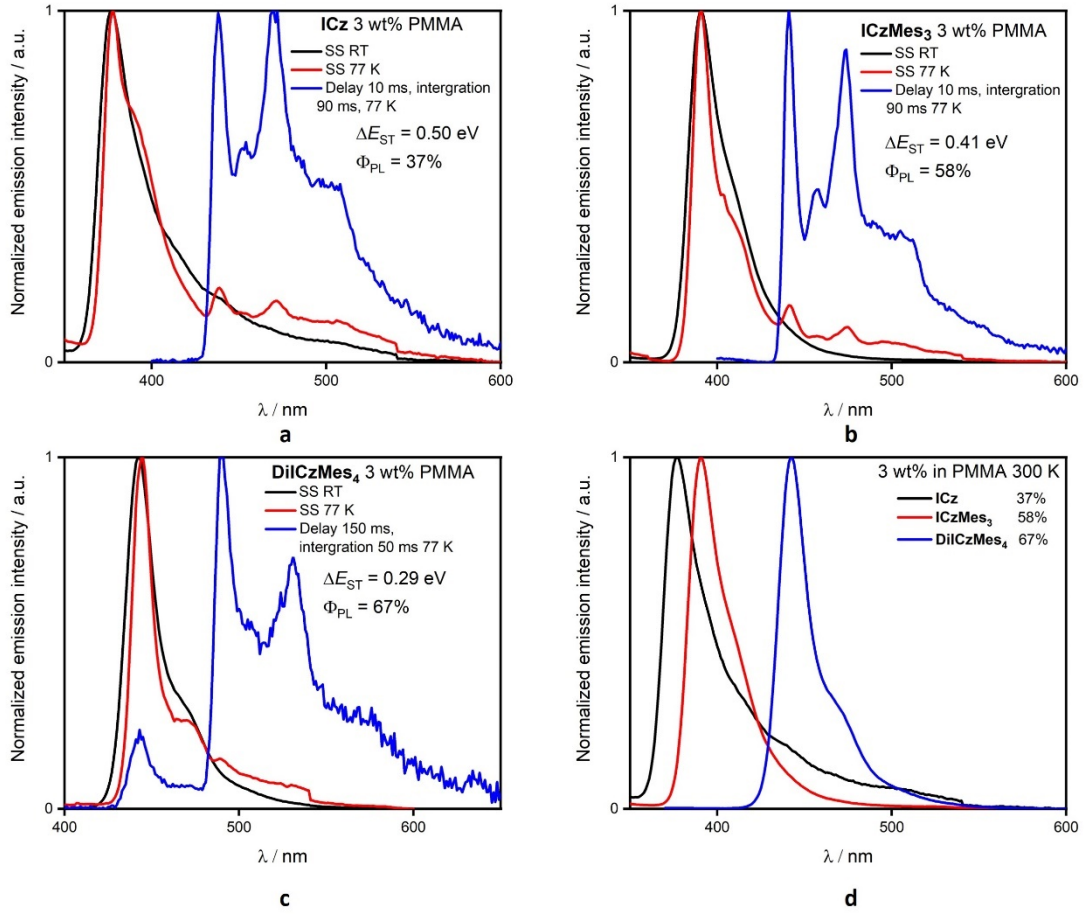

Figure **S36**. Solid-state photophysical data in 3 wt% PMMA, emission spectra (**a**, **c**, **e**) steady-state at RT, 77 K and gated emission, and stacked emission spectra. **ICz** (**a**), **ICzMes$_3$** (**b**), **DiICzMes$_4$** (**c**), λ_{exc} = 330 nm

#

Table **S16**. Concentration dependence of **DiICzMes$_4$** in mCP doped films.

Doping concentration in mCP / %[a]	**λ_{em} / nm**	**Φ_{PL} N_2 / %**	**Φ_{PL} Air / %**	**FWHM / nm (eV)**
1	456	82	48	33 (0.19)
3	457	82	44	40 (0.23)
5	459	77	48	41 (0.23)
7	459	76	57	42 (0.24)
10	461	71	47	42 (0.24)
15	461	62	49	47 (0.27)
20	467	57	37	48 (0.27)
Neat	502	30	19	56 (0.27)

[a]Dropcast films, λ_{exc} = 350 nm.

Table **S17**. Rates and efficiencies of **DiICzMes$_4$** in 3 wt% mCP at 300 K.

Compound	**Φ_p**	**Φ_d**	**k_p / × 10^7 s^{-1}**	**k_d / × 10^3 s^{-1}**	**k_{ISC} / × 10^7 s^{-1}**	**k_{RISC} / × 10^2 s^{-1}**
DiICzMes$_4$	0.808	0.123	7.4	2.3	1.4	1.8

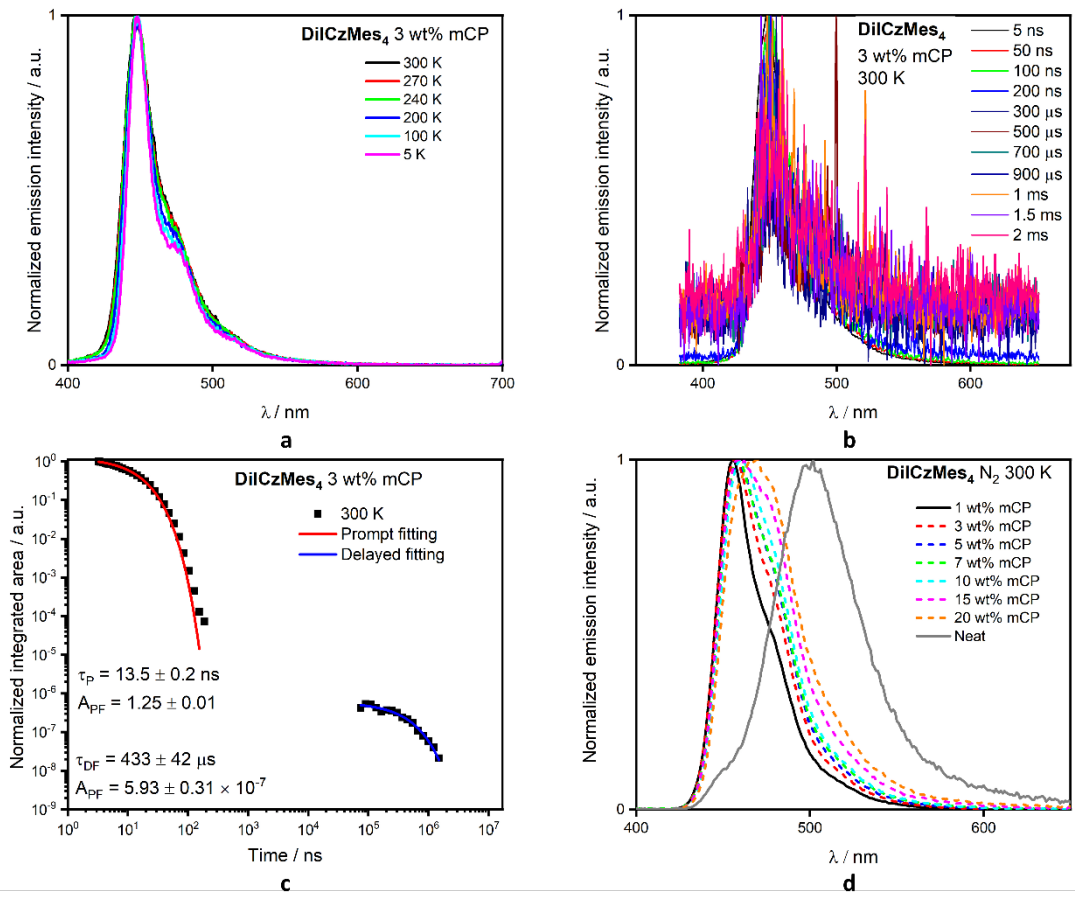

Figure **S37**. Solid state data of **DiICzMes4** in 3.5 wt% mCP, λ_{exc} = 355 nm, unless stated. **a)** prompt emission as a function of temperature, **b)** photoluminesence spectra at 300 K at different time delays, **c)** time-resolved PL at 300 K, **d)** steady-state PL at different doping concetrations in dropcast mCP films, λ_{exc} = 350 nm.

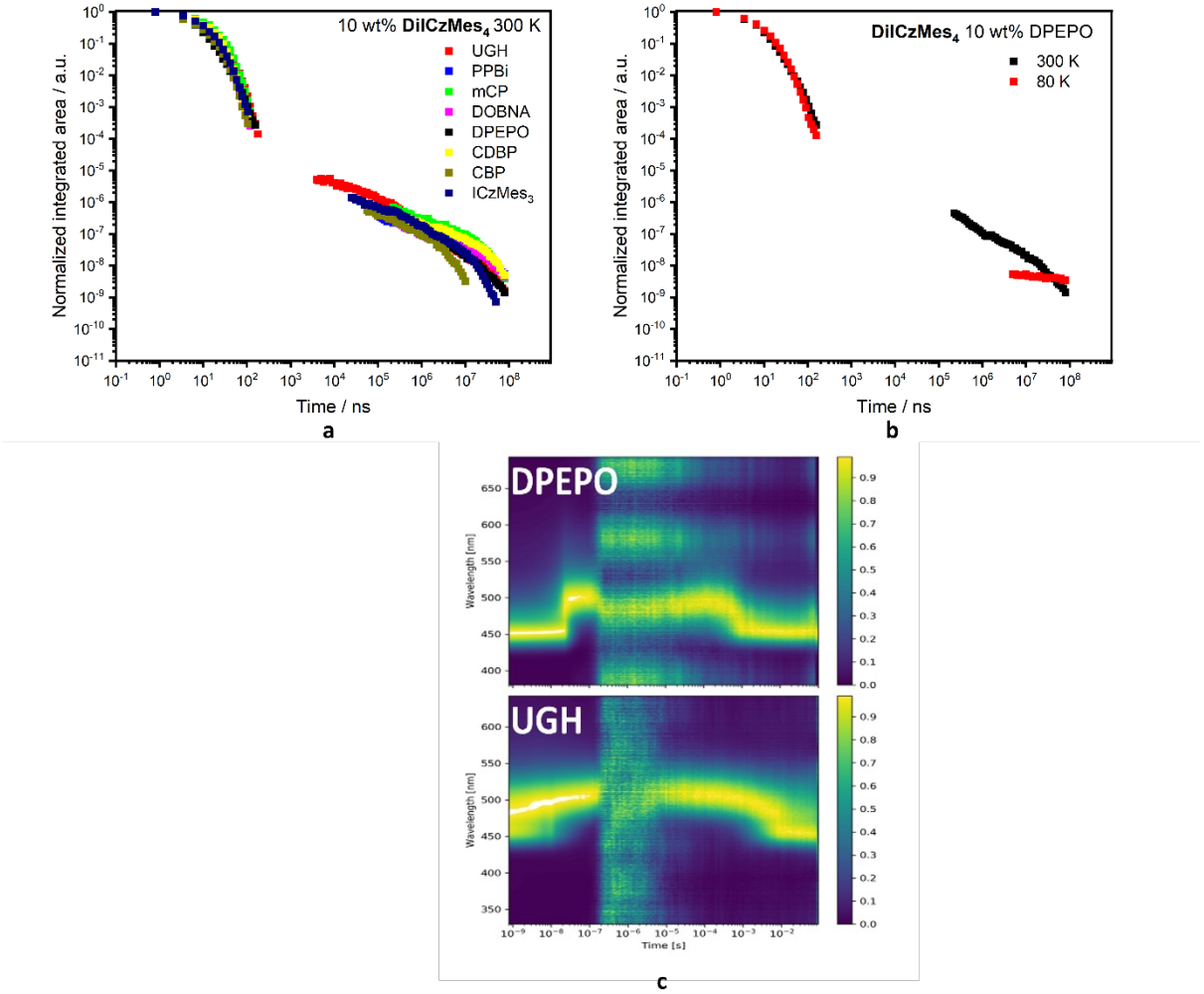

Figure **S38.** Time-resolved emission decays of **DiICzMes4** in a range of OLED hosts (10% drop cast films, (**a**) measured at room temperature, (**b**) time-resolved emission decays of **DiICzMes4** in 10 wt% DPEPO at various temperature and (**c**) contour plots of time-resolved PL spectra (right) in DPEPO (top) and UGH (bottom), demonstrating dimer/excimer contribution at intermediate times at this concentration. Spectra between 2×10^{-7} and 10^{-5} s represent the noise baseline of the CCD system, while monomer-like emission reappears at times beyond 10ms.

OLED Data

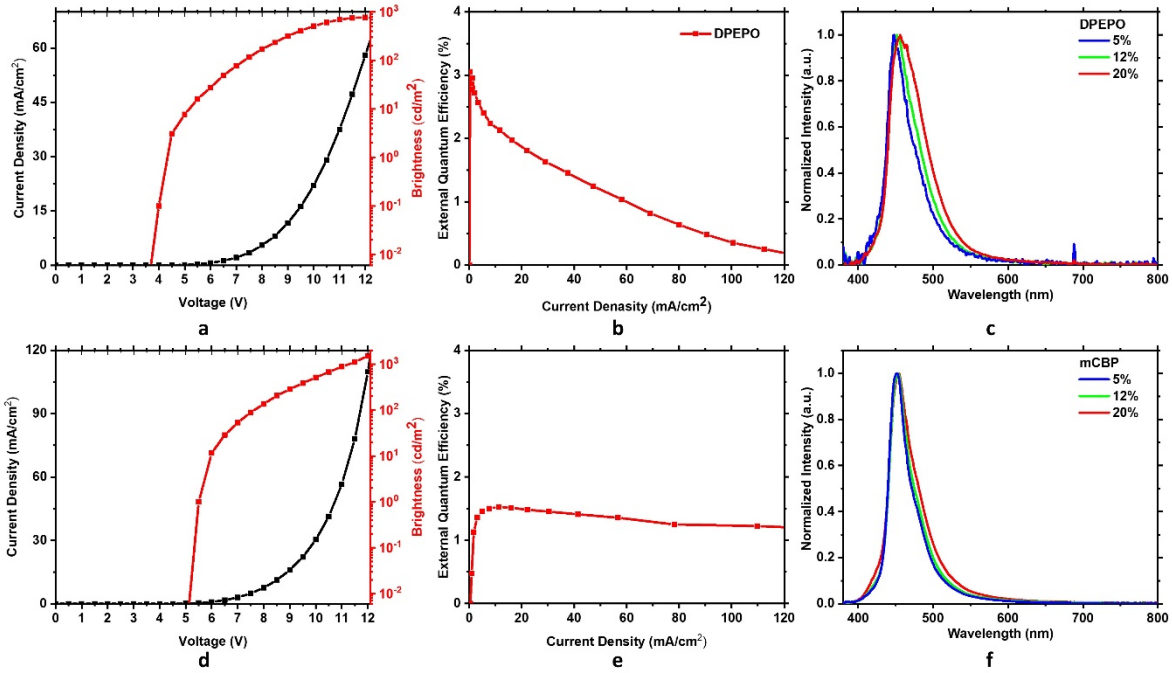

Figure **S39**. OLEDs performance of guest-host devices using **DiICzMes$_4$** as a guest, at 20% loading. (**a**) JVL, (**b**) EQE Vs current density and (**c**) EL spectra in different concentration of emitter in DPEPO host. (**d**) JVL, (**e**) EQE *vs* current density and (**f**) EL spectra in different concentration of emitter in mCBP host.

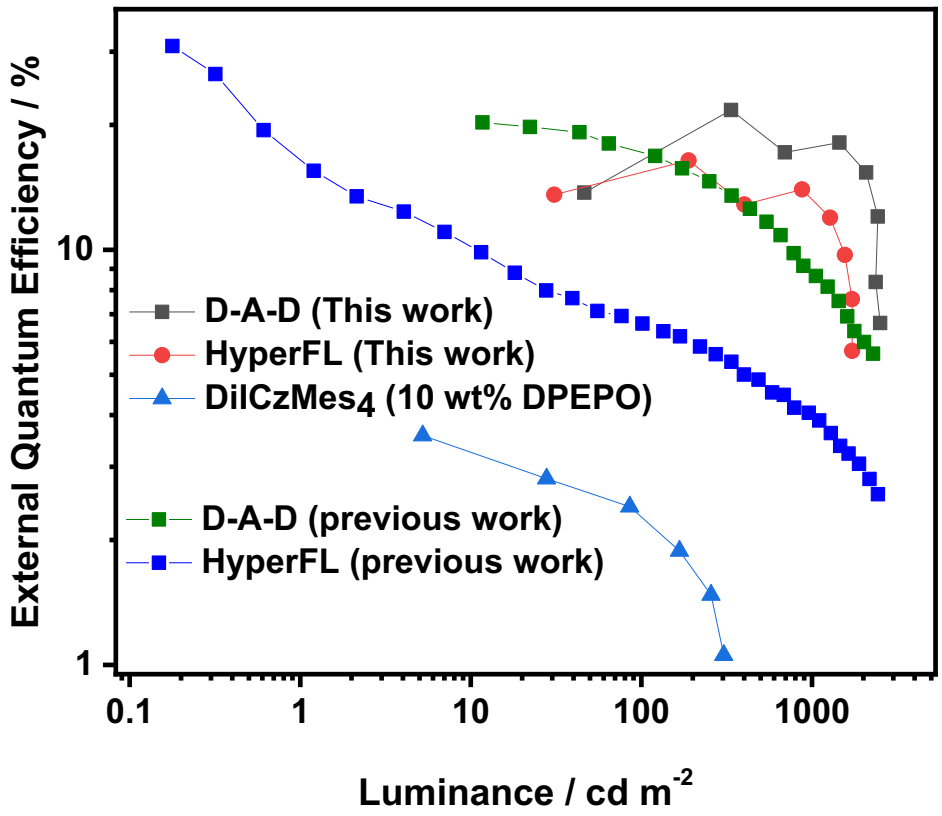

Figure **S40**. Comparison of D-A-D and hyperfluorescence OLED performance using different D-A-D cohosts (**DPAc-DtCzBN** data extracted from previous report[39]).

Table **S18**. Summary of previously reported deep blue HF-OLEDs.

Assistant dopant	Emitter	V_{on} / V	EQE_{max} / %	EQE_{100} / %	EQE_{1000} / %	Lum_{max} / cd/m^{-2}	CIE (x,y)	λ_{EL} / nm	Ref
DMAC2-TMXanSO2	**DiICzMes$_4$**	3.4	16.5	15.5	12.9	1500	0.15, 0.11	446	This work
DPAc-DtCzBN	**pICz**	3.5	32.0	6.7	4.0 [a]	2400 [a]	0.15, 0.10	445	39
DMAC-DPS	**tDABNA**	N/A	31.4	27.2	19.8	4800 [a]	0.13, 0.15	N/A	40
DMAC-DPS	**DABNA-1**	N/A	23.4 [a]	20.9 [a]	15.3 [a]	3800 [a]	0.14, 0.15	N/A	40
P4TCPhBN	**tDABNA**	N/A	32.5	30.6 [a]	23.2	N/A	0.13, 0.12	459 [a]	41
PCzTrz	**v-DABNA**	N/A	33.5	/	24.3	N/A	0.12, 0.18	473	42
HDT-1	**v-DABNA**	N/A	27	24	20	N/A	0.15, 0.20	470	43
DMAC2-TMXanSO2	**v-DABNA**	N/A	27.5	/	25.7 [a]	N/A	N/A	474 [a]	44
PtON7-dtb	**v-DABNA**	N/A	32.2	/	25.4	N/A	0.11, 0.14	473	45
DMAC-DMT	**BPPyA**	N/A	15.5	N/A	11.4 [b]	N/A	0.15, 0.11	N/A	46
CzAcSF	**TPBe**	N/A	17.2	N/a	12.4 [b]	N/A	0.14, 0.19	N/A	47
3CzBN-Cz	**Py-Cz**	4.1	10.2	N/A	N/A	6200	0.15, 0.14	468	48

[a] Data extracted from graphical fitting software; [b] Obtained at 500 cd m^{-2}.

References

1. N. G. Connelly and W. E. Geiger, *Chem. Rev.,* 1996, **96**, 877
2. C. M. Cardona, W. Li, A. E. Kaifer, D. Stockdale and G. C. Bazan, *Adv. Mater.,* 2011, **23**, 2367.
3. N. C. Greenham, I. D. W. Samuel, G. R. Hayes, R. T. Phillips, Y. A. R. R. Kessener, S. C. Moratti, A. B. Holmes and R. H. Friend, *Chem. Phys. Lett.,* 1995, **241**, 89.
4. M. J. Frisch, G. W. Trucks, H. B. Schlegel, G. E. Scuseria, M. A. Robb, J. R. Cheeseman, G. Scalmani, V. Barone, G. A. Petersson, H. Nakatsuji, X. Li, M. Caricato, A. V. Marenich, J. Bloino, B. G. Janesko, R. Gomperts, B. Mennucci, H. P. Hratchian, J. V. Ortiz, A. F. Izmaylov, J. L. Sonnenberg, Williams, F. Ding, F. Lipparini, F. Egidi, J. Goings, B. Peng, A. Petrone, T. Henderson, D. Ranasinghe, V. G. Zakrzewski, J. Gao, N. Rega, G. Zheng, W. Liang, M. Hada, M. Ehara, K. Toyota, R. Fukuda, J. Hasegawa, M. Ishida, T. Nakajima, Y. Honda, O. Kitao, H. Nakai, T. Vreven, K. Throssell, J. A. Montgomery Jr., J. E. Peralta, F. Ogliaro, M. J. Bearpark, J. J. Heyd, E. N. Brothers, K. N. Kudin, V. N. Staroverov, T. A. Keith, R. Kobayashi, J. Normand, K. Raghavachari, A. P. Rendell, J. C. Burant, S. S. Iyengar, J. Tomasi, M. Cossi, J. M. Millam, M. Klene, C. Adamo, R. Cammi, J. W. Ochterski, R. L. Martin, K. Morokuma, O. Farkas, J. B. Foresman and D. J. Fox *Gaussian 16 Rev. A.01*, Wallingford, CT, 2016.
5. A. Hellweg, S. A. Grun and C. Hattig, *Phys. Chem. Chem. Phys.,* 2008, **10**, 4119.
6. C. Hättig, *J. Chem. Phys.,* 2003, **118**, 7751.
7. J. Thorn H. Dunning, *J. Chem. Phys.,* 1989, **90**, 1007.
8. C. Hättig and F. Weigend, *J. Chem. Phys.,* 2000, **113**.
9. C. Hättig and K. Hald, *Phys. Chem. Chem. Phys.,* 2002, **4**, 2111.
10. C. Adamo and V. Barone, *J. Chem. Phys.,* 1999, **110**, 6158.
11. S. Hirata and M. Head-Gordon, *Chem. Phys. Lett.,* 1999, **314**, 291.
12. G. A. Petersson and M. A. Al-Laham, *J. Chem. Phys.,* 1991, **94**, 6081.
13. R Dennington, T. Keith and J. Millam *GaussView, Version 6.1.1*, KS: Semichem Inc.: Shawnee Mission, 2019.
14. K. Momma and F. Izumi, *J. Appl. Crystallogr.,* 2011, **44**, 1272.
15. T. Hatakeyama, K. Shiren, K. Nakajima, S. Nomura, S. Nakatsuka, K. Kinoshita, J. Ni, Y. Ono and T. Ikuta, *Adv. Mater.,* 2016, **28**, 2777.
16. Y. Kondo, K. Yoshiura, S. Kitera, H. Nishi, S. Oda, H. Gotoh, Y. Sasada, M. Yanai and T. Hatakeyama, *Nat. Photonics,* 2019, **13**, 678.
17. Y. Xu, Z. Cheng, Z. Li, B. Liang, J. Wang, J. Wei, Z. Zhang and Y. Wang, *Adv. Opt. Mater.,* 2020, **8**, 1902142.
18. M. Yang, I. S. Park and T. Yasuda, *J. Am. Chem. Soc.,* 2020, **142**, 19468.
19. Y. Zhang, D. Zhang, J. Wei, Z. Liu, Y. Lu and L. Duan, *Angew. Chem. Int. Ed.,* 2019, **58**, 16912.
20. Y. Zhang, D. Zhang, T. Huang, A. J. Gillett, Y. Liu, D. Hu, L. Cui, Z. Bin, G. Li, J. Wei and L. Duan, *Angew. Chem. Int. Ed.,* 2021.
21. S. Oda, B. Kawakami, R. Kawasumi, R. Okita and T. Hatakeyama, *Org. Lett.,* 2019, **21**, 9311.
22. J. A. Knoller, G. Meng, X. Wang, D. Hall, A. Pershin, D. Beljonne, Y. Olivier, S. Laschat, E. Zysman-Colman and S. Wang, *Angew. Chem. Int. Ed.,* 2020, **59**, 3156.
23. Y. Yuan, X. Tang, X. Y. Du, Y. Hu, Y. J. Yu, Z. Q. Jiang, L. S. Liao and S. T. Lee, *Adv. Opt. Mater.,* 2019, **7**, 1801536.
24. D. Hall, S. M. Suresh, P. L. dos Santos, E. Duda, S. Bagnich, A. Pershin, P. Rajamalli, D. B. Cordes, A. M. Z. Slawin, D. Beljonne, A. Köhler, I. D. W. Samuel, Y. Olivier and E. Zysman‐Colman, *Adv. Opt. Mater.,* 2020, **8**, 1901627.
25. K. Wang, X.-C. Fan, Y. Tsuchiya, Y.-Z. Shi, M. Tanaka, Z. Lin, Y.-T. Lee, X. Zhang, W. Liu, G.-L. Dai, J. Chen, B. Wu, J. Zhong, Jian-YuYuan, C.-J. Zheng, J. Yu, C. Lee, C. Adachi and X.-H. Zhang, *ChemRxiv. Preprint,* 2021, 10.26434/chemrxiv.13699057.v1.
26. N. Aizawa, A. Matsumoto and T. Yasuda, *Sci. Adv.,* 2021, **7**, eabe5769.
27. L.-S. Cui, A. J. Gillett, S.-F. Zhang, H. Ye, Y. Liu, X.-K. Chen, Z.-S. Lin, E. W. Evans, W. K. Myers, T. K. Ronson, H. Nakanotani, S. Reineke, J.-L. Bredas, C. Adachi and R. H. Friend, *Nat. Photonics,* 2020, **14**, 636.

28. Y. Wada, H. Nakagawa, S. Matsumoto, Y. Wakisaka and H. Kaji, *Nat. Photonics,* 2020, **14**, 643.
29. M. Nagata, H. Min, E. Watanabe, H. Fukumoto, Y. Mizuhata, N. Tokitoh, T. Agou and T. Yasuda, *Angew. Chem. Int. Ed.,* 2021, **60**, 20820.
30. Y. Xu, C. Li, Z. Li, Q. Wang, X. Cai, J. Wei and Y. Wang, *Angew. Chem. Int. Ed.,* 2020, **59**, 17442.
31. N. Ikeda, S. Oda, R. Matsumoto, M. Yoshioka, D. Fukushima, K. Yoshiura, N. Yasuda and T. Hatakeyama, *Adv. Mater.,* 2020, **32**, e2004072.
32. V. V. Patil, H. L. Lee, I. Kim, K. H. Lee, W. J. Chung, J. Kim, S. Park, H. Choi, W. J. Son, S. O. Jeon and J. Y. Lee, *Adv. Sci.,* 2021, e2101137.
33. L. Wang, E. Ji, N. Liu and B. Dai, *Synthesis,* 2016, **48**, 737.
34. J. Lv, Q. Liu, J. Tang, F. Perdih and K. Kranjc, *Tetrahedron Lett.,* 2012, **53**, 5248.
35. C. Zhao, T. Schwartz, B. Stoger, F. J. White, J. Chen, D. Ma, J. Frohlich and P. Kautny, *J. Mater. Chem. C.,* 2018, **6**, 9914.
36. C. Maeda, T. Todaka and T. Ema, *Org. Lett.,* 2015, **17**, 3090.
37. F. B. Dias, T. J. Penfold and A. P. Monkman, *Methods Appl. Fluoresc.,* 2017, **5**, 012001.
38. K. Masui, H. Nakanotani and C. Adachi, *Org. Electron.,* 2013, **14**, 2721.
39. J. Wei, C. Zhang, D. Zhang, Y. Zhang, Z. Liu, Z. Li, G. Yu and L. Duan, *Angew. Chem. Int. Ed.,* 2021, **60**, 12269.
40. S. H. Han, J. H. Jeong, J. W. Yoo and J. Y. Lee, *J. Mater. Chem. C.,* 2019, **7**, 3082.
41. D. Zhang, X. Song, A. J. Gillett, B. H. Drummond, S. T. E. Jones, G. Li, H. He, M. Cai, D. Credgington and L. Duan, *Adv. Mater.,* 2020, **32**, e1908355.
42. S. O. Jeon, K. H. Lee, J. S. Kim, S.-G. Ihn, Y. S. Chung, J. W. Kim, H. Lee, S. Kim, H. Choi and J. Y. Lee, *Nat. Photonics,* 2021, **15**, 208.
43. C.-Y. Chan, M. Tanaka, Y.-T. Lee, Y.-W. Wong, H. Nakanotani, T. Hatakeyama and C. Adachi, *Nat. Photonics,* 2021, **15**, 203.
44. K. Stavrou, A. Danos, T. Hama, T. Hatakeyama and A. Monkman, *ACS Appl. Mater. Interfaces,* 2021, **13**, 8643.
45. S. Nam, J. W. Kim, H. J. Bae, Y. M. Maruyama, D. Jeong, J. Kim, J. S. Kim, W. J. Son, H. Jeong, J. Lee, S. G. Ihn and H. Choi, *Adv. Sci.,* 2021, **8**, e2100586.
46. D. H. Ahn, J. H. Jeong, J. Song, J. Y. Lee and J. H. Kwon, *ACS Appl. Mater. Interfaces,* 2018, **10**, 10246.
47. I. H. Lee, W. Song, J. Y. Lee and S.-H. Hwang, *J. Mater. Chem. C.,* 2015, **3**, 8834.
48. D. Liu, K. Sun, G. Zhao, J. Wei, J. Duan, M. Xia, W. Jiang and Y. Sun, *J. Mater. Chem. C.,* 2019, **7**, 11005.